ASYMPTOTIC AND NUMERICAL ANALYSIS OF THE ALLEN-CAHN EQUATION WITH A MASS CONSTRAINT

By

Douglas James Stafford

B. Sc. University of British Columbia, 1995

A THESIS SUBMITTED IN PARTIAL FULFILLMENT OF

THE REQUIREMENTS FOR THE DEGREE OF

MASTER OF SCIENCE

in

THE FACULTY OF GRADUATE STUDIES

DEPARTMENT OF MATHEMATICS

INSTITUTE OF APPLIED MATHEMATIC

We accept this thesis as conforming

to the required standard

THE UNIVERSITY OF BRITISH COLUMBIA

August 1997

In presenting this thesis in partial fulfillment of the requirements for an advanced degree at the University of British Columbia, I agree that the Library shall make it freely available for reference and study. I further agree that permission for extensive copying of this thesis for scholarly purposes may be granted by the head of my department or by his or her representatives. It is understood that copying or publication of this thesis for financial gain shall not be allowed without my written permission.

Department of Mathematics
Institute of Applied Mathematic
The University of British Columbia
2075 Wesbrook Place
Vancouver, Canada
V6T 1Z1

Date:

1997-08-29

Abstract

The Allen-Cahn equation with a mass constraint is analyzed asymptotically and numerically in a two-dimensional domain. This problem models the phase separation of a binary mixture in the presence of a mass constraint. Solutions develop internal layers, or interfaces, that propagate depending on the curvature of the interfaces while keeping the area they enclose constant. Small interfaces attached to the boundary of the domain are shown to move along the boundary in the direction of increasing boundary curvature. The motion of the interfaces is simulated numerically to verify these asymptotic results. The slow motion behavior of a semi-circular interface intersecting a flat boundary segment is also analyzed. The projection method is used to derive an explicit ordinary differential equation for the location of the center of such a semi-circular interface.

Table of Contents

List of Tables

List of Figures

Acknowledgement

I would like to thank Michael Ward for his encouragement and assistance during the production of this thesis. I also thank Brian Wetton for providing the Fortran code that the numerics in this thesis are based on.

Chapter 1

Introduction

A simple model for problem of phase separation in a binary mixture is the Allen-Cahn equation with a mass constraint:

$$u_t = \epsilon^2 \Delta u + Q(u) - \sigma\,, \qquad \mathbf{x} \in D \subset \mathbf{R^2}\,, \tag{1.1a}$$

$$\partial_n u = 0\,, \qquad \mathbf{x} \in \partial D\,, \tag{1.1b}$$

$$\int_D u(\mathbf{x},t)\,d\mathbf{x} = M\,. \tag{1.1c}$$

Here $u = u(\mathbf{x},t)$ is the concentration of one of the two species, $\mathbf{x} = (x,y)$, $\epsilon \ll 1$, D is a bounded two-dimensional domain, and the mass M is constant. We assume that $Q(u) = -V'(u)$, where $V(u)$ is a double-well potential with wells of equal depth at $u = s_\pm$. Thus $Q(u)$ has three zeroes located at $u = s_- < 0$, $u = 0$, and $u = s_+ > 0$ and is taken to satisfy

$$Q(s_\pm) < 0\,, \quad Q(0) > 0\,, \quad V(s_+) = 0\,, \quad V(u) = -\int_{s_-}^{u} Q(\eta)\,d\eta. \tag{1.2}$$

To satisfy the mass constraint (1.1c), the function $\sigma = \sigma(t)$ is given by

$$\sigma = \frac{1}{|D|}\int_D Q(u)\,d\mathbf{x}\,. \tag{1.3}$$

In (1.3), $|D|$ is the total area of D. Notice that due to the form of σ, (1.1a) is a nonlocal reaction diffusion equation.

This problem has been well studied from several viewpoints (see [1], [13], [18]). The analysis in these papers have revealed many aspects of the dynamics of the solution to (1.1). Starting from arbitrary initial data, the solution develops internal layers, or interfaces, on an $O(1/\epsilon)$ time interval. These layers have width $O(\epsilon)$ and separate regions in which $u \sim s_-$ from regions in which $u \sim s_+$. The asymptotic analysis of Rubinstein and Sternberg in [13] as $\epsilon \to 0$ showed

that the normal velocity v of the interfaces, denoted by Γ, satisfies the area preserving mean curvature flow

$$v \sim \epsilon^2 \left(\kappa - \frac{1}{|\Gamma|} \int_\Gamma \kappa \, ds \right) . \tag{1.4}$$

Here κ is the curvature of Γ, $|\Gamma|$ is the total length of all interfaces, and $\int_\Gamma$ denotes integration over all interfaces. This holds for interfaces in the interior of D and for interfaces connected to ∂D with the added condition that the interface must intersect the boundary orthogonally. A single closed convex interface evolving according to (1.4) will tend to a circle enclosing the same area [9]. When there are several interfaces, interfaces enclosing large areas grow at the expense of smaller interfaces while preserving the total area enclosed by all interfaces [13]. This is referred to a a coarsening process. With appropriate initial data, this can lead to the case of a single closed circular interface inside the domain D. A numerical method has been used to simulate the dynamics of (1.4) for closed interfaces in [7]. For the case of a circular interface, or *bubble*, contained in D equation (1.4) gives no motion since $v = 0$ for a circle. Ward was able to show in [18] that a bubble solution to (1.1) drifts exponentially slowly towards the closest point on ∂D without a change in shape. Specifically, the distance between the center of the bubble and the closest point on the boundary of D, $r_m(t)$, satisfies the asymptotic ODE

$$r_m'(t) \sim -\frac{\epsilon^{3/2} \zeta r_m^{-1/2}}{(1 - K_m r_m)^{1/2}} e^{-2\nu_+^\epsilon \epsilon^{-1}(r_m - r_b)} . \tag{1.5}$$

Here K_m is the curvature of ∂D at the point closest to the circular interface (positive for a convex domain D), r_b is the bubble radius, and ζ and ν_+^ϵ are constants that depend on ϵ. When the distance between the interface and ∂D is $O(\epsilon)$, a fast transformation takes place resulting in an interface intersecting ∂D orthogonally. This interface remains connected to ∂D and it evolves according to (1.4) until a steady state is attained. When the length scale of an interface is sufficiently small compared to the radius of curvature of ∂D the interface will become approximately semi-circular in shape. Alikakos, Chen, and Fusco show in [1] that the center of such a small *drop* satisfies the following differential equation as $\delta \to 0$ subject to

$0 < \epsilon < \delta^3$:

$$\xi'(t) \sim \frac{4\epsilon^2\delta}{3\pi} K_D'(\xi(t))\,. \tag{1.6}$$

In (1.6), ξ is an arclength parameter for ∂D, δ is the radius of the drop, and K_D is the curvature of ∂D (positive for a convex domain D).

In this thesis, we derive some of the results stated above, simulate (1.4) numerically, and show a new result for the motion of a semi-circular interface along a flat boundary portion of ∂D. In §2 the method of matched asymptotic expansions is used in a multiple time scale setting to derive (1.4), the motion by area preserving mean curvature result. In §3 the derivation of (1.6), the asymptotic differential equation for the motion of a small drop along the domain boundary, is presented. Next, we use the numerical method of [7], modified for general domain boundary curves, to simulate motion of interfaces by (1.4) in §4. Numerical results are compared to known asymptotic results for closed interfaces and interfaces intersecting ∂D. In particular we compare the numerical motion of small interfaces along the domain boundary to (1.6). In §5 we apply the projection method developed by Ward ([17], [18]) to a metastable problem for the evolution of a straight line interface for the unconstrained Allen-Cahn equation. This result agrees with the results of [3] and [12]. Finally, we note that (1.4) gives no indication of the motion of a semi-circular interface intersecting a flat portion of the domain boundary. We examine this metastable problem in §6 for a domain with a straight-line boundary segment between $(x_L, 0)$ and $(x_R, 0)$. The projection method introduced in §5 is used to determine an explicit asymptotic ODE for the center of such a semi-circular interface, $x_0(t)$, as it moves slowly along the flat boundary portion of D. The ODE is found to be

$$\begin{aligned} x_0'(t) \;\sim\; & \frac{2\epsilon a_+^2 (\nu_+^\epsilon)^2}{\pi\beta} \left\{ \frac{K_R}{x_R - x_0} e^{-2\nu_+^\epsilon \epsilon^{-1}(x_R - x_0 - r_b)} \left(\frac{\epsilon}{2\nu_+^\epsilon}\right)^{\alpha_R+1} \Gamma(\alpha_R + 1) \right. \\ & \left. - \frac{K_L}{x_0 - x_L} e^{-2\nu_+^\epsilon \epsilon^{-1}(x_0 - x_L - r_b)} \left(\frac{\epsilon}{2\nu_+^\epsilon}\right)^{\alpha_L+1} \Gamma(\alpha_L + 1) \right\}. \end{aligned} \tag{1.7}$$

Here K_L, α_L and K_R, α_R are constants used to describe the shape of ∂D near $(x_L, 0)$ and $(x_R, 0)$ respectively. In addition, r_b is the radius of the semi-circular interface and a_+, ν_+^ϵ, and

β are constants that depend on ϵ and can be calculated asymptotically for a given $Q(u)$. Figure 1.1 depicts all of the types of motion of solutions to (1.1) described in this thesis after a single small closed convex interface has developed inside a particular domain D.

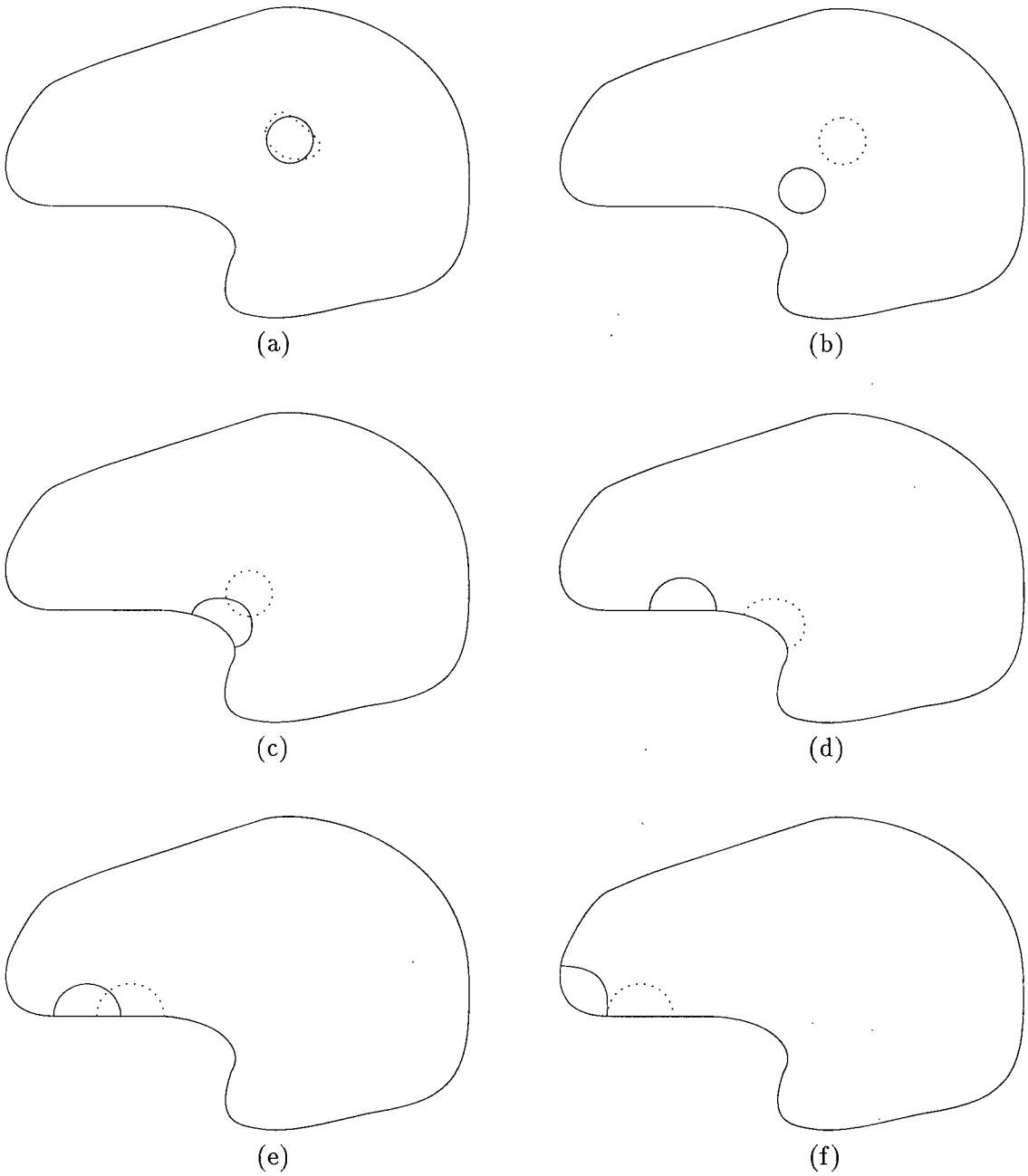

Figure 1.1: Evolution of a small convex interface inside a domain D. (a) The convex interface evolves by (1.4) into a circle. (b) The circular interface drifts, satisfying (1.5), towards the closest point on ∂D. (c) The interface attaches to ∂D, intersecting orthogonally. (d) The interface moves along ∂D satisfying (1.4). (e) If the interface encounters a flat portion of ∂D, it moves along this flat portion according to (1.7). (f) When a curved part of ∂D is reached, the interface again evolves by (1.4) until a steady state is attained.

Chapter 2

Area Preserving Motion by Curvature

In this chapter the solution to (1.1) is examined as $\epsilon \to 0$ to obtain the motion by area preserving mean curvature result, equation (1.4), first derived in [13]. We use the method of matched asymptotic expansions with multiple time scales in this analysis. For this problem, we introduce a *fast* time variable $t^* = t$, a *slow* time variable $\tau = \epsilon t$, and a *very slow* time variable $\eta = \epsilon^2 t$. Outer and inner solutions are obtained and analyzed to determine the motion of the internal layers of the solution as t^* and $\tau \to \infty$.

2.1 The Outer Solution

Using multiple time scales, we expand the solution to (1.1) and $\sigma(t)$ in the form

$$u(\mathbf{x}, t; \epsilon) = v_0(\mathbf{x}, t^*, \tau, \eta) + \epsilon v_1(\mathbf{x}, t^*, \tau, \eta) + O(\epsilon^2)\,, \tag{2.1}$$

$$\sigma(t; \epsilon) = \sigma_0(t^*, \tau, \eta) + \epsilon \sigma_1(t^*, \tau, \eta) + O(\epsilon^2)\,. \tag{2.2}$$

Substituting (2.1) in (1.1) and collecting powers of ϵ we obtain to leading order

$$(v_0)_{t^*} = Q(v_0) - \sigma_0\,, \tag{2.3a}$$

$$\partial_n v_0 = 0\,, \tag{2.3b}$$

$$\int_D v_0(\mathbf{x}, t^*, \tau, \eta)\, d\mathbf{x} = M\,. \tag{2.3c}$$

Thus $v_0(\mathbf{x}, t^*, \tau, \eta)$ approaches a steady state, $v_0(\mathbf{x}, \infty, \tau, \eta)$, in the limit $t^* \to \infty$. From (2.3a), this steady state satisfies

$$Q[v_0(\mathbf{x}, \infty, \tau, \eta)] = \sigma_0(\infty, \tau, \eta)\,. \tag{2.4}$$

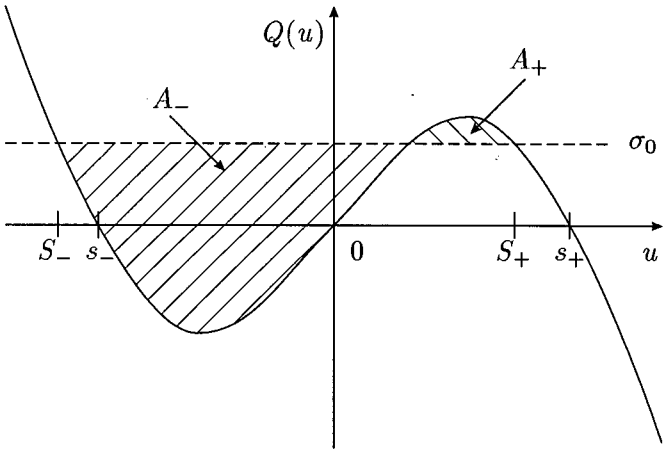

Figure 2.1: Plot of a typical function $Q(u)$. The values of $S_+(\tau,\eta)$ and $S_-(\tau,\eta)$ are shown for a given $\sigma_0(\infty,\tau,\eta)$. The hatched areas represent $A_+(\tau,\eta)$ and $A_-(\tau,\eta)$.

The steady state is of the following form:

$$v_0(\mathbf{x},\infty,\tau,\eta) = \begin{cases} S_-(\tau,\eta)\,, & \mathbf{x}\in D_{s_-}(\tau,\eta)\,, \\ S_+(\tau,\eta)\,, & \mathbf{x}\in D_{s_+}(\tau,\eta)\,, \end{cases} \tag{2.5}$$

where

$$D_{s_-}(\tau,\eta)\cup D_{s_+}(\tau,\eta) = D\,, \tag{2.6}$$

$$S_-(\tau,\eta)|D_{s_-}(\tau,\eta)| + S_+(\tau,\eta)|D_{s_+}(\tau,\eta)| = M\,. \tag{2.7}$$

Here $S_-(\tau,\eta)$ and $S_+(\tau,\eta)$ are the leftmost and rightmost roots of (2.4) respectively. (See Figure 2.1.) Thus, we have obtained that as $t^*\to\infty$, the domain D is divided into subdomains, D_{s_-} and D_{s_+}, with v_0 approaching a value independent of $\mathbf{x}$ in each subdomain. This outer solution satisfies the boundary condition (1.1b) to leading order. The solution is assumed to have a layered structure so that (2.7) represents the leading order approximation to the mass constraint (1.1c).

2.2 The Inner Solution

Separating the subdomains are internal layers or interfaces in which u has large gradients. To determine the asymptotic behavior of u near these interfaces we construct an inner solution. We refer to the interfaces as $\Gamma(\tau,\eta)$ and describe their location in terms of a function $\phi(\mathbf{x},\tau,\eta)$. At $\tau=0$, ϕ is the signed distance from $\mathbf{x}\in D$ to the interface and we set $\phi>0$ for $\mathbf{x}\in D_{s_+}$. Then, near an interface we use the following expansion:

$$u(\mathbf{x},t;\epsilon)=u_0(z,\mathbf{x},t^*,\tau,\eta)+\epsilon u_1(z,\mathbf{x},t^*,\tau,\eta)+O(\epsilon^2)\,, \tag{2.8}$$

where

$$z=\phi(\mathbf{x},\tau,\eta)/\epsilon\,. \tag{2.9}$$

Substituting (2.8) in (1.1a) and collecting powers of ϵ we obtain that u_0 and u_1 satisfy

$$(u_0)_{t^*}+\phi_\tau(u_0)_z-(\nabla\phi)^2(u_0)_{zz}-Q(u_0)+\sigma_0(\infty,\tau,\eta)=0\,, \tag{2.10}$$

$$\begin{aligned}(u_1)_{t^*}+\phi_\tau(u_1)_z-(\nabla\phi)^2(u_1)_{zz}+Q'(u_0)u_1-\sigma_1(\infty,\tau,\eta)=\\ -(u_0)_\tau+(\Delta\phi)(u_0)_z+2\nabla\phi\cdot\nabla(u_0)_z-\phi_\eta(u_0)_z\,.\end{aligned} \tag{2.11}$$

We assume for large t^* that u_0 and u_1 tend to travelling waves. Then we set

$$u_0(z,\mathbf{x},t^*,\tau,\eta)\sim F(z-ct^*,\mathbf{x},\tau,\eta)\quad\text{as } t^*\to\infty\,, \tag{2.12}$$

$$u_1(z,\mathbf{x},t^*,\tau,\eta)\sim G(z-ct^*,\mathbf{x},\tau,\eta)\quad\text{as } t^*\to\infty\,. \tag{2.13}$$

Here c is the constant speed of the waves. Using (2.12) and (2.13) in (2.10) and (2.11) we find that F and G satisfy the differential equations

$$(\phi_\tau-c)F'-(\nabla\phi)^2F''-Q(F)+\sigma_0(\infty,\tau,\eta)=0\,, \tag{2.14}$$

$$(\phi_\tau-c)G'-(\nabla\phi)^2G''-Q'(F)G+\sigma_1(\infty,\tau,\eta)=-F_\tau+(\Delta\phi)F'+2\nabla\phi\cdot\nabla(F')-\phi_\eta F'\,. \tag{2.15}$$

In (2.14) and (2.15), the primes represent differentiations with respect to z. To match to the outer solution in (2.5), we have that F tends to $S_-(\tau,\eta)$ as $z\to-\infty$ and to $S_+(\tau,\eta)$ as $z\to\infty$.

Then we multiply (2.14) by F', integrate the result from $z = -\infty$ to $z = \infty$, and rearrange to obtain

$$\begin{aligned} \phi_\tau - c &= \frac{V[S_-(\tau,\eta)] - V[S_+(\tau,\eta)] - \sigma_0(\infty,\tau,\eta)\,[S_+(\tau,\eta) - S_-(\tau,\eta)]}{\int_{-\infty}^{\infty}(F')^2\,dz} \\ &= \frac{A_+(\tau,\eta) - A_-(\tau,\eta)}{\int_{-\infty}^{\infty}(F')^2\,dz}\,. \end{aligned} \tag{2.16}$$

Here we have used $V(u)$ defined in (1.2). We also use the notation here that $A_-(\tau,\eta)$ represents the area of the region above the graph of $Q(u)$ and below the line $\sigma_0(\infty,\tau,\eta)$ and $A_+(\tau,\eta)$ represents the area of the region below the graph of $Q(u)$ and above the line $\sigma_0(\infty,\tau,\eta)$. (See Figure 2.1.) To determine the evolution of the interfaces on the τ time scale, we use the function

$$\psi(\mathbf{x},\tau,\eta) = \phi(\mathbf{x},\tau,\eta) - c\tau\,. \tag{2.17}$$

The location of the interface is then determined by the zero set of ψ. We use the new variable s and the function $R(s,\tau,\eta)$ defined by

$$s = \frac{z - ct^*}{|\nabla\psi|}\,, \qquad R(s,\tau,\eta) = F(z - ct^*, \mathbf{x}, \tau, \eta)\,. \tag{2.18}$$

We substitute (2.18) in (2.14) and (2.16) to determine that

$$R_{ss} - \frac{A_+(\tau,\eta) - A_-(\tau,\eta)}{\int_{-\infty}^{\infty}(R_s)^2\,ds}R_s + Q(R) - \sigma_0(\infty,\tau,\eta) = 0\,, \tag{2.19a}$$

$$R(-\infty,\tau,\eta) = S_-(\tau,\eta)\,, \qquad R(\infty,\tau,\eta) = S_+(\tau,\eta)\,, \tag{2.19b}$$

and

$$\frac{\psi_\tau}{|\nabla\psi|} = \frac{A_+(\tau,\eta) - A_-(\tau,\eta)}{\int_{-\infty}^{\infty}(R_s)^2\,ds}\,. \tag{2.20}$$

To interpret the motion determined by (2.20), we notice that $\psi_\tau/|\nabla\psi|$ is just the normal velocity of a level set of ψ. Then (2.20) is an equation for the normal velocity of the interfaces on the τ time scale. We differentiate (2.7) with respect to τ to find that

$$(S_-)_\tau|D_{s_-}(\tau,\eta)| + S_-|D_{s_-}|_\tau + (S_+)_\tau|D_{s_+}| + S_+|D_{s_+}|_\tau = 0\,. \tag{2.21}$$

When $A_- < A_+$, (2.20) gives $\psi_\tau > 0$. Thus the interfaces are propagating is such a way so that D_{s_-} is decreasing is size while D_{s_+} increases. In this situation we have $|D_{s_-}|_\tau < 0$, $|D_{s_+}|_\tau > 0$

and from (1.2) we know that $S_- < 0$ and $S_+ > 0$. Putting this information into (2.21), we find that S_- and S_+ must both decrease. Referring to Figure 2.1 we see that $\sigma_0(\infty, \tau, \eta)$ must increase for this to be true. This causes A_- to grow and A_+ gets reduced. Similarly, when $A_- > A_+$, the interfaces move to decrease A_- and increase A_+. So, as $\tau \to \infty$, S_+ and S_- approach values such that $A_- = A_+$. From (1.2) we see that this can only happen if $S_\pm(\infty, \eta) = s_\pm$ and $\sigma_0(\infty, \infty, \eta) = 0$. Summarizing our results, as $\tau \to \infty$ we have

$$v_0(\mathbf{x}, \infty, \infty, \eta) = \begin{cases} s_-\,, & \mathbf{x} \in D_{s_-}(\infty, \eta)\,, \\ s_+\,, & \mathbf{x} \in D_{s_+}(\infty, \eta)\,, \end{cases} \tag{2.22}$$

$$\frac{\psi_\tau}{|\nabla\psi|} = \frac{A_+(\infty, \eta) - A_-(\infty, \eta)}{\int_{-\infty}^{\infty}(R_s)^2\, ds} = 0\,. \tag{2.23}$$

Note that we have found that v_0, σ_0, $S_\pm$, and $A_\pm$ are all independent of η.

Next we find the motion of the interfaces on the η time scale. As $\tau \to \infty$ we use $\phi_\tau - c = \psi_\tau = 0$, and $F_\tau = 0$ in (2.15) to find that G satisfies

$$-(\nabla\phi)^2 G'' - Q'(F)G = (\Delta\phi + 2\nabla\phi \cdot \nabla)F' - \phi_\eta F' - \sigma_1(\infty, \infty, \eta)\,. \tag{2.24}$$

We multiply (2.24) by F' and integrate from $z = -\infty$ to $z = \infty$. Two integrations by parts can be used to show that the left side of this equation can be written as

$$-\int_{-\infty}^{\infty} \left[(\nabla\psi)^2 F''' + Q'(F)F'\right] G\, dz\,. \tag{2.25}$$

Differentiating (2.14) with respect to z as $\tau \to \infty$ we find

$$(\nabla\psi)^2 F''' + Q'(F)F' = 0\,. \tag{2.26}$$

Therefore the left side of our result equals zero and using $\phi_\eta = \psi_\eta$, $\nabla\phi = \nabla\psi$, and $\Delta\phi = \Delta\psi$, the remaining terms can be rearranged to obtain

$$\psi_\eta = \Delta\psi + \frac{\left[\nabla\psi \cdot \nabla \int_{-\infty}^{\infty}(F')^2\, dz - \sigma_1(\infty, \infty, \eta)(s_+ - s_-)\right]}{\int_{-\infty}^{\infty}(F')^2\, dz}\,. \tag{2.27}$$

We write this in terms of R and s using (2.18) and get

$$\psi_\eta = \Delta\psi + |\nabla\psi| \left[\nabla\psi \cdot \nabla\left(\frac{1}{|\nabla\psi|}\right) - \gamma(\eta)\right], \tag{2.28}$$

where

$$\gamma(\eta) = \frac{\sigma_1(\infty, \infty, \eta)(s_+ - s_-)}{\int_{-\infty}^{\infty}(R_s)^2\, ds}\,. \tag{2.29}$$

Here we use that the normal velocity on the η time scale, v, and mean curvature, κ, of a level set of ψ are given by $v = \psi_\eta/|\nabla\psi|$ and $\kappa = \nabla\cdot(\nabla\psi/|\nabla\psi|)$. Then we use (2.28) to show that on the η time scale, the interfaces $\Gamma(\mathbf{x}, \infty, \eta)$, given by $\{\mathbf{x} : \psi(\mathbf{x}, \infty, \eta) = 0\}$ evolve according to

$$v = \kappa - \gamma\,. \tag{2.30}$$

To determine γ we use (2.6), (2.7), and (2.22) to obtain that as $\tau \to \infty$,

$$|D_{s_-}| + |D_{s_+}| = |D|\,, \tag{2.31}$$

$$s_-|D_{s_-}| + s_-|D_{s_-}| = M\,. \tag{2.32}$$

Taking the η derivative of (2.31) and (2.32) we find that the following condition must hold:

$$|D_{s_-}|_\eta = |D_{s_+}|_\eta = 0\,. \tag{2.33}$$

Next we use the identity [13]

$$|D_{s_+}|_\eta = \int_\Gamma v\, ds\,. \tag{2.34}$$

We substitute (2.30) into (2.34) and use (2.33) to solve for γ:

$$\gamma = \frac{1}{|\Gamma|}\int_\Gamma \kappa\, ds\,. \tag{2.35}$$

Here $|\Gamma|$ is the total length of the interfaces. Finally, the normal velocity of the interfaces on the η time scale is obtained by putting (2.35) in (2.30):

$$v = \kappa - \frac{1}{|\Gamma|}\int_\Gamma \kappa\, ds\,. \tag{2.36}$$

2.3 Summary and Extensions

In this section we write out results in terms of the original time variable, t. We have shown that starting from initial data, as $\epsilon t \to \infty$, the solution to (1.1) develops interfaces, Γ, separating

regions where $u \sim s_+$ from regions where $u \sim s_-$. (See Figure 2.2.) The subsequent evolution is such that the normal velocity, v, of the interfaces is governed by

$$v = \epsilon^2 \left(\kappa - \frac{1}{|\Gamma|} \int_\Gamma \kappa \, ds \right) + O(\epsilon^3) . \tag{2.37}$$

Note that from (2.9), (2.17), and (2.18) we have as $t \to \infty$ that

$$u(\mathbf{x}, t; \epsilon) \sim R \left(\frac{\psi(\mathbf{x}, \epsilon t, \epsilon^2 t)}{\epsilon |\nabla \psi|} \right) . \tag{2.38}$$

If an interface has an endpoint on ∂D, we apply the boundary condition (1.1b) to (2.38) to obtain that on ∂D,

$$R' \left(\frac{\psi(\mathbf{x}, \epsilon t, \epsilon^2 t)}{\epsilon |\nabla \psi|} \right) \partial_n \left(\frac{\psi(\mathbf{x}, \epsilon t, \epsilon^2 t)}{\epsilon |\nabla \psi|} \right) = 0 . \tag{2.39}$$

Since the interface is given by $\{\mathbf{x} : \psi(\mathbf{x}, \epsilon t, \epsilon^2 t) = 0\}$, (2.39) reduces to

$$\partial_n \psi(\mathbf{x}, \epsilon t, \epsilon^2 t) = 0 , \qquad \mathbf{x} \in \partial D \cap \{\mathbf{x} : \psi(\mathbf{x}, \epsilon t, \epsilon^2 t) = 0\} . \tag{2.40}$$

This shows that when an interface intersects the boundary, it intersects orthogonally.

From (2.33) we see that the motion of the interfaces by (2.37) keeps the area enclosed by the interfaces constant. Because of this, the flow (2.37) is referred to as motion by area preserving mean curvature. Several other properties of this motion are derived in [9] and [13]. In [9], Gage shows that (2.37) shortens the length of the interfaces as time evolves and that a single closed convex interface converges to a circle as $t \to \infty$. In addition, from [13], when there are multiple interfaces a coarsening process occurs in which interfaces enclosing large areas grow at the expense of those enclosing smaller areas until only one circular interface remains. These results have been verified numerically in [7] and in Chapter 4.

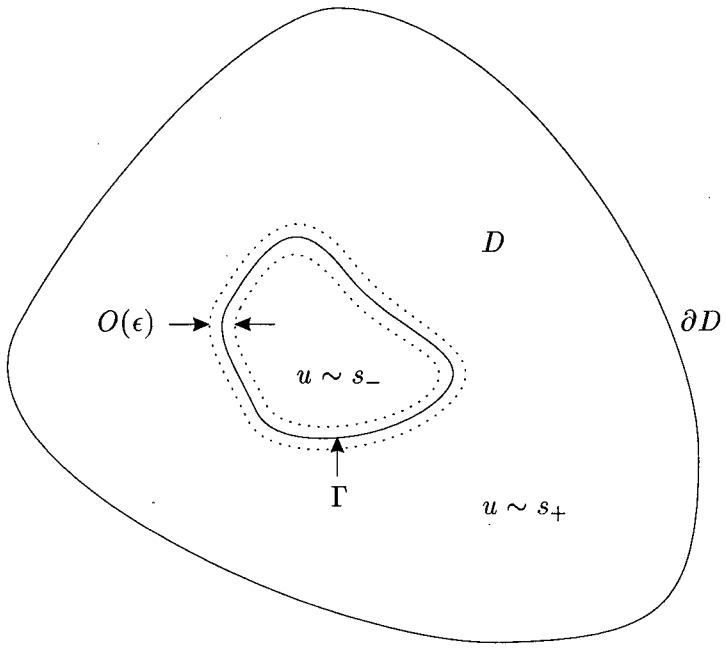

Figure 2.2: Plot of a solution to (1.1) that has developed a single closed interface. The interface evolves according to (2.37).

Chapter 3

Motion of a Small Drop Along the Boundary

In this chapter we consider the evolution of a single small interface intersecting the domain boundary. If the length scale of the interface is relatively small compared to the radius of curvature of the domain boundary the results of Chapter 2 suggest that the shape of this interface will become approximately semi-circular while intersecting ∂D at right angles. Since evolution by (1.4) shortens the length of interfaces, we expect that this *drop* will move along the domain boundary in the direction where the curvature of ∂D is increasing the most. This should continue until the drop attains a steady state surrounding a point on ∂D where the boundary curvature is a local maximum.

We examine the motion of such small drops using the procedure in [1]. To do this we consider the situation in which the solution to (1.1) is a drop solution. That is, u has developed a single small approximately semi-circular interface centered at $z(\xi)$ with radius $\delta \ll 1$ and intersecting ∂D orthogonally. Here ∂D is parameterized by $z(\xi)$ where ξ is a counterclockwise arclength parameter and we assume that the curvature of ∂D is $O(1)$. We take $u \sim s_-$ inside and $u \sim s_+$ outside of the drop. We also assume that the shape of the interface remains approximately semi-circular as it moves along the boundary so that $u(\mathbf{x},t) = \hat{u}(\mathbf{x},\xi(t))$ and $\sigma(t) = \epsilon\hat{\sigma}(\xi(t))$. The function $\xi = \xi(t)$ represents the arclength coordinate of the center of the semi-circular drop on ∂D. Writing $\xi'(t) = \epsilon^2 c(\xi)$ and using (1.1), we take $\hat{u}$ to satisfy

$$\epsilon^2\Delta\hat{u} + Q(\hat{u}) - \epsilon\hat{\sigma} - \epsilon^2 c\hat{u}_\xi = 0\,, \qquad \mathbf{x} \in D \subset \mathbf{R^2}\,, \tag{3.1a}$$

$$\partial_n\hat{u} = 0\,, \qquad \mathbf{x} \in \partial D\,, \tag{3.1b}$$

$$\int_D \hat{u}(\mathbf{x},\xi)\,d\mathbf{x} = s_+|D| - (s_+ - s_-)\pi\delta^2/2\,. \tag{3.1c}$$

Here $|D|$ is the area of D and we have used the result from Chapter 2 that as $t \to \infty$ then

$\sigma = O(\epsilon)$. We also assume that δ satisfies

$$0 < \epsilon \ll \delta^3 \ll 1\,. \tag{3.2}$$

As shown in [1], the condition $0 < \epsilon \ll \delta^3$ guarantees that a semi-circular interface is the least-energy solution and hence the drop will maintain its shape and will not spread out on the boundary. We use (3.1) to find conditions on the shape of the interface, $\Gamma(\xi)$, as $\epsilon \to 0$. Next, we solve (3.1) as $\delta \to 0$ subject to (3.2) to determine $c(\xi)$ and produce an asymptotic ODE for the motion of a drop along ∂D.

3.1 The ϵ-Series Expansion

In the region near the interface we introduce the local coordinates $\rho(\mathbf{x},\xi)$ and $s(\mathbf{x},\xi)$. We set $\rho = \epsilon^{-1}r$, where $-r$ is the distance from $\mathbf{x}$ inside the drop to $\Gamma(\xi)$, and we let s be a coordinate orthogonal to r. When $r = 0$, s is a counterclockwise arclength parameter for $\Gamma(\xi)$. In these coordinates we have

$$\epsilon^2\Delta_{\mathbf{x}} = \partial_{\rho\rho} + \epsilon\kappa(1+\epsilon\rho\kappa)^{-1}\partial_\rho + \epsilon^2(1+\epsilon\rho\kappa)^{-2}\partial_{ss} - \epsilon^3\rho\kappa_s(1+\epsilon\rho\kappa)^{-3}\partial_s\,, \tag{3.3a}$$

$$\partial_\xi = \epsilon^{-1}r_\xi\partial_\rho + s_\xi\partial_s + \partial_\xi\,. \tag{3.3b}$$

Here $\kappa(s,\xi)$ is the curvature of $\Gamma(\xi)$. In this region we use the following expansions:

$$\hat{u}(\mathbf{x},\xi;\epsilon) = \hat{u}_0(\rho) + \sum_{j=1}^{\infty}\epsilon^j\hat{u}_j(\rho,s,\xi)\,, \tag{3.4a}$$

$$\hat{\sigma}(\xi;\epsilon) = \sum_{j=0}^{\infty}\epsilon^j\hat{\sigma}_j(\xi)\,, \tag{3.4b}$$

$$Q(\hat{u}) = Q(\hat{u}_0) + \epsilon Q'(\hat{u}_0)\hat{u}_1 + O(\epsilon^2)\,, \tag{3.4c}$$

$$\kappa(s,\xi;\epsilon) = \sum_{j=0}^{\infty}\epsilon^j\kappa_j(s,\xi)\,, \tag{3.4d}$$

$$c(\xi;\epsilon) = \sum_{j=0}^{\infty}\epsilon^j c_j(\xi)\,, \tag{3.4e}$$

$$r_\xi(\mathbf{x},\xi;\epsilon) = \sum_{j=0}^{\infty}\epsilon^j r_j^\xi(\rho,s,\xi)\,, \tag{3.4f}$$

$$s_\xi(\mathbf{x},\xi;\epsilon) \;=\; \sum_{j=0}^{\infty} \epsilon^j s_j^\xi(\rho,s,\xi)\,. \tag{3.4g}$$

Substituting (3.3) and (3.4) into (3.1a) and collecting powers of ϵ, we get the leading order problem as $\epsilon \to 0$

$$\hat{u}_0'' + Q(\hat{u}_0) = 0\,, \quad -\infty < \rho < \infty\,. \tag{3.5}$$

To match to the outer solution, we require

$$\hat{u}_0 \sim s_\pm\,, \quad \text{as } \rho \to \pm\infty\,. \tag{3.6}$$

The first order problem is given by

$$L\hat{u}_1 \equiv (\hat{u}_1)_{\rho\rho} + Q'(\hat{u}_0)\hat{u}_1 = \left(\kappa_0 - c_0 r_0^\xi\right)\hat{u}_0' + \hat{\sigma}_0\,. \tag{3.7}$$

Differentiating (3.5) we see that $\hat{u}_0$ satisfies $L\hat{u}_0' = 0$. Thus we obtain the solvability condition that $(L\hat{u}_1, \hat{u}_0') = 0$ where $(u,v) \equiv \int_{-\infty}^{\infty} uv\,d\rho$. Applying this solvability condition to (3.7) yields

$$\kappa_0 - c_0 r_0^\xi + a_0\hat{\sigma}_0 = 0\,, \tag{3.8}$$

where

$$a_0 \equiv \frac{s_+ - s_-}{\int_{-\infty}^{\infty}(\hat{u}_0')^2\,d\rho}\,. \tag{3.9}$$

Summarizing, we have obtained, as $\epsilon \to 0$, that $\hat{u}$ is given asymptotically by

$$\hat{u}(\mathbf{x},\xi(t)) = \begin{cases} s_+ + O(\epsilon)\,, & \mathbf{x} \in D_{s_+}\,,\ \rho \neq O(1)\,, \\ \hat{u}_0(\rho) + O(\epsilon)\,, & \rho = O(1)\,, \\ s_- + O(\epsilon)\,, & \mathbf{x} \in D_{s_-}\,,\ \rho \neq O(1)\,. \end{cases} \tag{3.10}$$

In (3.10) D_{s_-} and D_{s_+} are the regions inside and outside of the drop respectively. Since we have assumed that Γ intersects ∂D orthogonally, (3.10) satisfies the boundary condition (3.1b) to leading order. In addition, the following expression is satisfied asymptotically

$$\kappa - cr_\xi + a_0\hat{\sigma} = O(\epsilon)\,. \tag{3.11}$$

To represent ∂D, as in [1] it is convenient to use to a complex valued function $\mathbf{z}(\xi) = (z^1(\xi) + iz^2(\xi))$ where ξ is a counterclockwise arclength parameter. Then the boundary is given

by $\partial D = \{(z^1(\xi), z^2(\xi)) : 0 \le \xi \le |\partial D|\}$ where $|\partial D|$ is the length of ∂D. If we let $\mathbf{z}'(\xi) = e^{i\phi(\xi)}$ where $\phi(\xi)$ is a known real valued function representing the angle between ∂D and the positive x-axis, then we have $\phi'(\xi) = K_D(\xi)$. Here $K_D(\xi)$ is the curvature of ∂D at ξ which we assume to be $O(1)$. We use the sign convention that K_D is positive if D is convex. Similarly we describe the location of the interface, $\Gamma(\xi)$, by a complex function $\mathbf{w}(s,\xi) = (w^1(s,\xi) + iw^2(s,\xi))$ so that $\Gamma(\xi) = \{(w^1(s,\xi), w^2(s,\xi)) : 0 \le s \le |\Gamma(\xi)|\}$ where $|\Gamma(\xi)|$ is the length of $\Gamma(\xi)$. Then there is a real function $\psi(s,\xi)$ such that [1]

$$\mathbf{w}_s(s,\xi) = e^{i[\psi(s,\xi)+\phi(\xi)+\pi/2]}. \tag{3.12}$$

Using this, the curvature of the interface is given by

$$\kappa(s,\xi) = \psi_s(s,\xi). \tag{3.13}$$

Since the interface is close to a semi-circle of radius δ we expect that $\kappa = O(\delta^{-1})$.

The interface and the domain boundary must intersect at two places. Thus, using the notation above we have

$$\mathbf{w}(0,\xi) = \mathbf{z}(\xi + g(\xi)), \tag{3.14a}$$

$$\mathbf{w}(|\Gamma(\xi)|,\xi) = \mathbf{z}(\xi - g(\xi)). \tag{3.14b}$$

Here $g(\xi)$ is a positive function and since $\Gamma(\xi)$ is close to a small semi-circle, we expect that $g = O(\delta)$. To satisfy (3.12) and (3.14a) we take $\mathbf{w}(s,\xi)$ in the form

$$\mathbf{w}(s,\xi) = \mathbf{z}(\xi + g(\xi)) + \int_0^s e^{i[\psi(\tilde{s},\xi)+\phi(\xi)+\pi/2]}\, d\tilde{s}. \tag{3.15}$$

Then to satisfy (3.14b) we require

$$\int_0^{|\Gamma(\xi)|} e^{i[\psi(\tilde{s},\xi)]}\, d\tilde{s} = i\int_{-g(\xi)}^{g(\xi)} e^{i[\phi(\xi+\zeta)-\phi(\xi)]}\, d\zeta. \tag{3.16}$$

We have assumed that the interface and the domain boundary intersect orthogonally so that $\hat{\mathbf{n}} \cdot \hat{\mathbf{N}} = 0$ at the intersection points. Here $\hat{\mathbf{n}}$ is the outward unit normal to $\Gamma(\xi)$ and $\hat{\mathbf{N}}$

is the outward unit normal to ∂D. Using the expressions for $\mathbf{w}$ and $\mathbf{z}$ above, these vectors are given by

$$\hat{\mathbf{n}} = e^{i[\psi(s,\xi)+\phi(\xi)]}, \qquad \hat{\mathbf{N}} = e^{i[\phi(\xi)-\pi/2]}. \tag{3.17}$$

Thus at the intersection points we have

$$\sin\left(\psi(0,\xi) + \phi(\xi) - \phi(\xi+g)\right) = 0\,, \tag{3.18a}$$

$$\sin\left(\psi(|\Gamma|,\xi) + \phi(\xi) - \phi(\xi-g)\right) = 0\,. \tag{3.18b}$$

Then from (3.18) we then have that ψ satisfies

$$\psi(0,\xi) = \phi(\xi + g(\xi)) - \phi(\xi)\,, \tag{3.19a}$$

$$\psi(|\Gamma|,(\xi)) = \pi + \phi(\xi - g(\xi)) - \phi(\xi)\,. \tag{3.19b}$$

We can convert (3.11) into a differential equation for $\psi(s,\xi)$ using (3.13). To do this we need to express r_ξ in terms of ψ. The relationship between r and $\mathbf{x}$ is

$$\mathbf{x} = \mathbf{w}(s,\xi) + r(\mathbf{x},\xi)\hat{\mathbf{n}}\,. \tag{3.20}$$

Differentiating (3.20) with respect to ξ we get

$$r_\xi(\mathbf{x},\xi) = -\mathbf{w}_\xi \cdot \hat{\mathbf{n}}\,. \tag{3.21}$$

Substituting (3.15) and (3.17) into (3.21) we obtain

$$r_\xi = -(1+g_\xi)\cos\left(\phi(\xi+g) - \phi(\xi) - \psi\right) + \int_0^s \left[\psi_\xi(\tilde{s},\xi) + \phi_\xi(\xi)\right]\cos\left(\psi(\tilde{s},\xi) - \psi(s,\xi)\right) d\tilde{s}\,. \tag{3.22}$$

Now (3.11) can be written as

$$\begin{aligned}\psi_s(s,\xi) \;=\; & -a_0\hat{\sigma} - c(1+g_\xi)\cos\left(\phi(\xi+g) - \phi(\xi) - \psi(s,\xi)\right) \\ & + c\int_0^s \left[\psi_\xi(\tilde{s},\xi) + \phi_\xi(\xi)\right]\cos\left(\psi(\tilde{s},\xi) - \psi(s,\xi)\right) d\tilde{s} + O(\epsilon)\,.\end{aligned} \tag{3.23}$$

To asymptotically evaluate the mass constraint (3.1c) we decompose it as

$$\int_D u(\mathbf{x},\xi)\, d\mathbf{x} = s_+(|D| - |D_{s_-}|) + s_-|D_{s_-}| + \int_{D_{s_+}} (\hat{u} - s_+)\, d\mathbf{x} + \int_{D_{s_-}} (\hat{u} - s_-)\, d\mathbf{x} + O(\epsilon)\,. \tag{3.24}$$

Here $|D_{s_-}|$ and $|D_{s_+}|$ are the areas of D_{s_-} and D_{s_+}. Using (3.10) we can evaluate the integrals in (3.24) as $\epsilon \to 0$ since dominant contributions to these integrals arise from the regions near the interface. Thus we obtain

$$\int_D u(\mathbf{x},\xi)\,d\mathbf{x} = s_+|D| - (s_+ - s_-)|D_{s_-}| + O(\epsilon)\,. \tag{3.25}$$

Now from the mass constraint condition, (3.1c), we get

$$|D_{s_-}| = \pi\delta^2/2 + O(\epsilon)\,. \tag{3.26}$$

Next we can calculate $|D_{s_-}|$ using

$$|D_{s_-}| = \frac{1}{2}\int_{\partial D_{s_-}} (x\,dy - y\,dx) = -\frac{1}{2}\Im\left\{\int_{\partial D_{s_-}} \mathbf{z}\,d\overline{\mathbf{z}}\right\} = -\frac{1}{2}\Im\left\{\int_{\partial D_{s_-}} [\mathbf{z} - \mathbf{z}(\xi+g)]\,d\overline{\mathbf{z}}\right\}. \tag{3.27}$$

Here $\Im$ denotes the imaginary part of a complex function and we have used that the integral of $\mathbf{z}(\xi+g)$ over ∂D_{s_-} is zero since ∂D_{s_-} is a closed curve. Using our expressions for $\mathbf{z}$ and $\mathbf{w}$ we then obtain

$$\begin{aligned}|D_{s_-}| &= -\frac{1}{2}\Im\left\{\int_{\xi-g}^{\xi+g}[\mathbf{z}(\tilde\xi) - \mathbf{z}(\xi+g)]\overline{\mathbf{z}'(\tilde\xi)}\,d\tilde\xi + \int_0^{|\Gamma|}[\mathbf{w}(\tilde s,\xi) - \mathbf{w}(0,\xi)]\overline{\mathbf{w}_s(\tilde s,\xi)}\,d\tilde s\right\}\\ &= -\frac{1}{2}\left\{\int_{\xi-g}^{\xi+g}\int_{\xi+g}^{\tilde\xi}\sin(\phi(\hat\xi) - \phi(\tilde\xi))\,d\hat\xi\,d\tilde\xi + \int_0^{|\Gamma|}\int_0^{\tilde s}\sin(\psi(\hat s,\xi) - \psi(\tilde s,\xi))\,d\hat s\,d\tilde s\right\}. \end{aligned}\tag{3.28}$$

Substituting (3.28) into (3.26) we obtain that ψ satisfies

$$\int_{\xi-g}^{\xi+g}\int_{\xi+g}^{\tilde\xi}\sin(\phi(\tilde\xi) - \phi(\hat\xi))\,d\hat\xi\,d\tilde\xi + \int_0^{|\Gamma|}\int_0^{\tilde s}\sin(\psi(\tilde s,\xi) - \psi(\hat s,\xi))\,d\hat s\,d\tilde s = \pi\delta^2 + O(\epsilon)\,. \tag{3.29}$$

3.2 The δ-Series Expansion

In this section we expand all of the unknown coefficients in powers of δ and proceed to solve (3.16), (3.19), (3.23), and (3.29) as $\delta \to 0$. These equations are now contain double series expansions. Since we have assumed that $0 < \epsilon < \delta^3 \ll 1$, the various terms in the equations can be ordered using $\delta^{-1} \gg 1 \gg \delta \gg \delta^2 \gg \delta^3 \gg \epsilon$. Specifically, we use the following

expansions:

$$\psi(s,\xi;\epsilon) = \delta^{-1}\sum_{j=0}^{\infty}\delta^j\psi_j(s,\xi)\,, \tag{3.30a}$$

$$g(\xi;\delta) = \sum_{j=0}^{\infty}\delta^j g_j(\xi)\,, \tag{3.30b}$$

$$|\Gamma(\xi;\delta)| = \sum_{j=0}^{\infty}\delta^j L_j(\xi)\,, \tag{3.30c}$$

$$\hat{\sigma}(\xi;\delta) = \delta^{-1}\sum_{j=0}^{\infty}\delta^j\hat{\sigma}_j(s,\xi)\,, \tag{3.30d}$$

$$c(\xi;\delta) = \sum_{j=0}^{\infty}\delta^j c_j(\xi)\,. \tag{3.30e}$$

In addition, we expand $\phi(\xi+\zeta)$ in a Taylor expansion as

$$\phi(\xi+\zeta) = \phi(\xi) + K_D(\xi)\zeta + \frac{1}{2}K_D'(\xi)\zeta^2 + \cdots\,. \tag{3.31}$$

In (3.31) $K_D(\xi)$ is the curvature of ∂D at ξ. To simplify the calculations, we assume throughout that $g = O(\delta)$, $g_\xi = O(\delta^2)$, $\hat{\sigma} = O(\delta^{-1})$, and $c = O(\delta)$. Also note that all calculations done here are valid up to $O(\epsilon)$ but we suppress writing this in each equation.

First we solve the differential equation (3.23) with the initial condition (3.19a) up to $O(\delta)$:

$$\psi(s,\xi) = \phi(\xi+g(\xi)) - \phi(\xi) - a_0\hat{\sigma}s + O(\delta^2)\,. \tag{3.32}$$

Here we have assumed that the terms containing c in (3.23) are $O(\delta^2)$. Substituting this back into (3.23), we can solve up to $O(\delta^2)$ to obtain

$$\psi(s,\xi) = \phi(\xi+g) - \phi(\xi) - a_0\hat{\sigma}s + c\left[-\frac{\sin(a_0\hat{\sigma}s)}{a_0\hat{\sigma}} + K_D\frac{1-\cos(a_0\hat{\sigma}s)}{(a_0\hat{\sigma})^2}\right] + O(\delta^3)\,. \tag{3.33}$$

To satisfy (3.19b) we require

$$a_0\hat{\sigma}|\Gamma| = -\pi + \phi(\xi+g) - \phi(\xi-g) + c\left[-\frac{\sin(a_0\hat{\sigma}|\Gamma|)}{a_0\hat{\sigma}} + K_D\frac{1-\cos(a_0\hat{\sigma}|\Gamma|)}{(a_0\hat{\sigma})^2}\right] + O(\delta^3)\,. \tag{3.34}$$

Using (3.31), the Taylor expansions of sin and cos about $-\pi$, and the assumptions that $g = O(\delta)$ and $c = O(\delta)$ we can show that the term containing c in (3.34) is $O(\delta^3)$. Thus we can write (3.34) as

$$a_0\hat{\sigma}|\Gamma| = -\pi + 2K_D g + O(\delta^3)\,. \tag{3.35}$$

Next we need that ψ satisfies (3.16). Using (3.31), the right side can be evaluated as

$$\begin{aligned} i\int_{-g}^{g} e^{i[\phi(\xi+\zeta)-\phi(\xi)]}\,d\zeta &= i\int_{-g}^{g}\left[1+i(K_D\zeta+\frac{1}{2}K_D'\zeta^2+\cdots)-\frac{1}{2}(K_D\zeta+\cdots)^2+\cdots\right]d\zeta \\ &= 2gi+\frac{1}{3}\left(iK_D^2-K_D'\right)g^3+O(\delta^4)\,. \end{aligned} \tag{3.36}$$

Using (3.33) the left side of (3.16) becomes

$$\begin{aligned} \int_0^{|\Gamma|} e^{i\psi}\,ds &= A(\xi,g)\int_0^{|\Gamma|} e^{-ia_0\hat{\sigma}s}\left\{1+ic\left[-\frac{\sin(a_0\hat{\sigma}|\Gamma|)}{a_0\hat{\sigma}}+K_D\frac{1-\cos(a_0\hat{\sigma}|\Gamma|)}{(a_0\hat{\sigma})^2}\right]+O(\delta^3)\right\}ds \\ &= A(\xi,g)e^{i[\phi(\xi+g)-\phi(\xi)]}\left\{\frac{e^{-ia_0\hat{\sigma}|\Gamma|}-1}{-ia_0\hat{\sigma}}+ic\left(\frac{e^{-2ia_0\hat{\sigma}|\Gamma|}-1}{4(a_0\hat{\sigma})^2}+\frac{i|\Gamma|}{2a_0\hat{\sigma}}\right)\right. \\ &\quad \left.+icK_D\left(\frac{e^{-ia_0\hat{\sigma}|\Gamma|}-1}{-i(a_0\hat{\sigma})^3}-\frac{|\Gamma|}{2(a_0\hat{\sigma})^2}+\frac{e^{-2ia_0\hat{\sigma}|\Gamma|}-1}{4(a_0\hat{\sigma})^3}\right)\right\}+O(\delta^4)\,, \end{aligned} \tag{3.37}$$

where

$$A(\xi,g)\equiv e^{i[\phi(\xi+g)-\phi(\xi)]}\,. \tag{3.38}$$

We can evaluate (3.37) using (3.31), (3.34), Taylor expansions and assuming that $g=O(\delta)$ and $\hat{\sigma}=O(\delta^{-1})$ to obtain

$$\int_0^{|\Gamma|} e^{i\psi}\,ds=\frac{1}{a_0\hat{\sigma}}\left[K_D'g^2-c\frac{|\Gamma|}{2}+i(-2+K_D^2g^2)\right]+O(\delta^4)\,. \tag{3.39}$$

Equating the real and imaginary parts of (3.36) and (3.39) we get

$$c=\tfrac{2K_D'g^2}{|\Gamma|}(1+\tfrac{1}{3}a_0\hat{\sigma}g)+O(\delta^4)\,, \tag{3.40}$$

$$a_0\hat{\sigma}g=-2+K_D^2g^2(1-\tfrac{1}{3}a_0\hat{\sigma}g)+O(\delta^3)\,. \tag{3.41}$$

Finally we solve (3.29). Using a Taylor expansion and (3.31) we can express first term on the left side of (3.29) as

$$\begin{aligned} \int_{\xi-g}^{\xi+g}\int_{\xi+g}^{\tilde{\xi}}\sin(\phi(\tilde{\xi})-\phi(\hat{\xi}))\,d\hat{\xi}\,d\tilde{\xi} &= \int_{-g}^{g}\int_{g}^{\zeta}\sin(\phi(\xi+\zeta)-\phi(\xi+\hat{\zeta}))\,d\hat{\zeta}\,d\zeta \\ &= \int_{-g}^{g}\int_{g}^{\zeta}\left[K_D(\zeta-\hat{\zeta})+\frac{1}{2}K_D'(\zeta^2-\hat{\zeta}^2)+\cdots\right]d\hat{\zeta}\,d\zeta \\ &= \frac{4}{3}K_Dg^3+O(\delta^4)\,. \end{aligned} \tag{3.42}$$

Here we have again assumed that $g = O(\delta)$. Similarly the second term on the left side of (3.29) becomes

$$\begin{aligned}\int_0^{|\Gamma|}\int_0^{\tilde{s}} \sin(\psi(\tilde{s},\xi)-\psi(\hat{s},\xi))\,d\hat{s}\,d\tilde{s} &= \int_0^{|\Gamma|}\int_0^{\tilde{s}} \sin\left[a_0\hat{\sigma}(\hat{s}-\tilde{s})+O(\delta^2)\right]\,d\hat{s}\,d\tilde{s}\\ &= \frac{\sin(a_0\hat{\sigma}|\Gamma|)-a_0\hat{\sigma}|\Gamma|}{(a_0\hat{\sigma})^2}+O(\delta^4)\\ &= \frac{\pi-4K_Dg}{(a_0\hat{\sigma})^2}+O(\delta^4)\,. \end{aligned} \tag{3.43}$$

Here we have used $c = O(\delta)$, $\sigma = O(\delta^{-1})$, and (3.34). Substituting these expressions into (3.29) we obtain

$$(a_0\hat{\sigma})^2\pi\delta^2 = \pi - 4K_Dg(1-\frac{1}{3}(a_0\hat{\sigma})^2g^2)+O(\delta^2)\,. \tag{3.44}$$

We now use the δ-series expansions, (3.30), in equations (3.35), (3.40), (3.41), and (3.44) to determine $\hat{\sigma}$, g, $|\Gamma|$, and c. To leading order, equation (3.44) produces

$$\hat{\sigma}_0 = -a_0^{-1}\,. \tag{3.45}$$

In (3.45) we have used from (3.35) that $\hat{\sigma} < 0$ since $|\Gamma|$ and a_0 are positive. Using this result in (3.41) we get

$$g_0 = 0\,, \tag{3.46}$$

$$g_1 = 1\,. \tag{3.47}$$

Substituting (3.45) in (3.35) we find

$$L_0 = \pi\delta\,. \tag{3.48}$$

Finally, we use these results in equation (3.40) to obtain

$$c_0 = 0\,, \tag{3.49}$$

$$c_1 = \frac{4}{3\pi}K_D'\,. \tag{3.50}$$

Note that we have found that $g = O(\delta)$, $g_\xi = O(\delta^2)$, $\hat{\sigma} = O(\delta^{-1})$, and $c = O(\delta)$ which is what we assumed to simplify the calculations.

3.3 Summary and Alternate Derivation

Using the results of the previous section, we have obtained an ordinary differential equation for the location of the center of a small drop moving along the domain boundary. This ODE is satisfied asymptotically as $\delta \to 0$ for $0 < \epsilon \ll \delta^3$ and is given by

$$\xi'(t) = \frac{4\epsilon^2\delta}{3\pi} K_D'(\xi(t)) + O(\epsilon^2\delta^3)\,. \tag{3.51}$$

Recall that $K_D(\xi)$ is the curvature of ∂D at ξ. Thus according to (3.51), the drop will move in the direction of increasing curvature of ∂D as expected and attain a steady state at a local maximum of the boundary curvature. We note that while we have used the condition $0 < \epsilon \ll \delta^3$ to order the terms in our double series expansion, this restriction is necessary. It is shown in [1] that if δ is smaller than an $O(\epsilon^{1/3})$ critical size, a constant solution to (1.1) is more energy efficient than a small drop solution. Because of this drop solutions will not occur for very small δ.

The result (3.51) can also be directly derived from (1.4) without any reference to (1.1). To do this we use the same notation for $\mathbf{w}(s,\xi)$ and $\mathbf{z}(\xi)$ introduced in §3.1. The endpoint condition, equation (3.16), must still be satisfied. The interface intersects the boundary at right angles, so (3.19) is needed. We also assume that the interface encloses an area of $\pi\delta^2$ so that (3.29) is satisfied. Next, instead of deriving (3.23) using (3.1), we assume that the interface evolves by (1.4) so that

$$c\mathbf{w}_\xi = \mathbf{w}_{ss} - \frac{1}{|\Gamma|}\left(\int_\Gamma \mathbf{w}_{ss}\cdot\hat{\mathbf{n}}\,ds\right)\hat{\mathbf{n}} + O(\epsilon)\,. \tag{3.52}$$

This is because the projection of (3.52) in the direction of $\hat{\mathbf{n}}$ produces (1.4). Substituting (3.15), (3.17), and $\mathbf{z}'(\xi) = e^{i\phi(\xi)}$ into (3.52) we obtain

$$\begin{aligned} c(1+g_\xi)e^{i\phi(\xi+g)} - c\int_0^s [\psi_\xi(\hat{s},\xi)+\phi_\xi(\xi)]e^{i[\psi(\hat{s},\xi)+\phi(\xi)]}\,d\hat{s} = \\ -\psi_s(s,\xi)e^{i[\psi(s,\xi)+\phi(\xi)]} + \frac{1}{|\Gamma|}[\psi(|\Gamma|,\xi)-\psi(0,\xi)]e^{i[\psi(s,\xi)+\phi(\xi)]} + O(\epsilon)\,. \end{aligned} \tag{3.53}$$

We multiply this by $e^{-i[\psi(s,\xi)+\phi(\xi)]}$, take the real part and rearrange terms to get that $\psi(s,\xi)$

satisfies the asymptotic differential equation

$$\begin{aligned}\psi_s(s,\xi) &= \frac{1}{|\Gamma|}[\psi(|\Gamma|,\xi)-\psi(0,\xi)] - c(1+g_\xi)\cos\left(\phi(\xi+g)-\phi(\xi)-\psi(s,\xi)\right) \\ &\quad + c\int_0^s [\psi_\xi(\tilde{s},\xi)+\phi_\xi(\xi)]\cos\left(\psi(\tilde{s},\xi)-\psi(s,\xi)\right)\,d\tilde{s} + O(\epsilon)\,. \end{aligned} \tag{3.54}$$

Now we can solve (3.16), (3.19), (3.29), and (3.54) as in §3.2 to obtain (3.51). Note that using (3.19) and (3.34) we obtain that

$$[\psi(|\Gamma|,\xi)-\psi(0,\xi)] = \pi + \phi(\xi-g)-\phi(\xi+g) = -a_0\hat{\sigma}|\Gamma| + O(\delta^3)\,. \tag{3.55}$$

Thus (3.23) and (3.54) give the same differential equation for ψ.

Chapter 4

Numerical Motion by Area Preserving Mean Curvature

In this chapter we model the Allen-Cahn equation numerically . Specifically, we examine a numerical model for the normal velocity of the interfaces developed by solutions to (1.1) as $\epsilon t \to \infty$. If there are several interfaces in the domain, the normal velocity of the i^{th} interface, Γ_i, is determined from the motion by area preserving mean curvature result (1.4):

$$v_i \sim \epsilon^2 \left(\kappa_i - \frac{1}{|\Gamma|} \sum_i \int_{\Gamma_i} \kappa_i \, ds \right) . \tag{4.1}$$

Here v_i is the normal velocity of Γ_i, κ_i is the curvature of Γ_i, and $|\Gamma|$ is the total length of all interfaces [13]. To be consistent with the definitions in Chapter 2, we use the sign convention that when Γ_i is convex, v_i is in the outward normal direction and κ_i is negative. If an interface intersects the boundary it must intersect orthogonally.

This chapter is organized as follows. In §4.1 a numerical method based on the method of lines for computing motion by area preserving mean curvature is described. Some numerical results are presented in §4.2. These numerical results are compared to asymptotic properties of solutions to the Allen-Cahn equation presented in Chapter 1. In particular, we examine the numerical evolution of approximately semi-circular interfaces intersecting ∂D. The radii of these semi-circular interfaces, called *drops*, are assumed to be small compared to the radius of curvature ∂D. We then compare the numerical motion of these small drops to the asymptotic result for the Allen-Cahn equations derived in Chapter 3 which states that

$$\xi'(t) \sim \frac{4\epsilon^2 \delta}{3\pi} K_D'(\xi(t)), \tag{4.2}$$

where $\delta \to 0$ and $0 < \epsilon \ll \delta^3$. Here ξ is an arc length parameter for ∂D, δ is the radius of the drop, and K_D is the curvature of ∂D. We use the sign convention that K_D is positive for a convex domain.

4.1 Numerical Model for Motion by Area Preserving Mean Curvature

In this section, we set up a discretization scheme based on [7] for modelling motion by curvature as given by (4.1). A front tracking method is used. First, partial differential equations that describe motion by curvature are presented. We then apply the method of lines to these equations, discretizing in space and stepping forward in time.

4.1.1 Equations of Motion

To eliminate the dependence on ϵ, we use the change of variables, $\tau = \epsilon^2 t$. We assume that the interfaces, Γ_i, are described parametrically by $\mathbf{x}^i(\sigma,\tau) = (x^i(\sigma,\tau), y^i(\sigma,\tau))$ where $\sigma \in [0,1]$. In this situation, a partial differential equation that describes the motion given by (4.1) is

$$\mathbf{x}^i_\tau = \frac{\mathbf{x}^i_{\sigma\sigma}}{|\mathbf{x}^i_\sigma|^2} - \frac{1}{|\Gamma|}\left(\sum_i \int_{\Gamma_i} \frac{\mathbf{x}^i_{\sigma\sigma}}{|\mathbf{x}^i_\sigma|^2} \cdot \hat{\mathbf{n}}_i \, ds\right) \hat{\mathbf{n}}_i \,, \tag{4.3}$$

where $\hat{\mathbf{n}}_i$ is a unit normal to Γ_i. It is easily seen that the projection of (4.3) in the normal direction of a given interface agrees with equation (4.1). Note that (4.1) is arbitrary up to any velocity in the tangential direction.

If the interfaces are closed curves, then we have

$$\mathbf{x}^i(0,\tau) = \mathbf{x}^i(1,\tau)\,. \tag{4.4}$$

If the interfaces intersect the boundary, then they intersect at a normal angle. Thus if the boundary, ∂D, is parameterized by $\mathbf{z}(\xi)$, where ξ is an arclength parameter, then this boundary condition can be written as

$$\mathbf{x}^i_\sigma(0,\tau) \cdot \mathbf{z}'(\xi^i_0(\tau)) = 0\,, \tag{4.5a}$$

$$\mathbf{x}^i_\sigma(1,\tau) \cdot \mathbf{z}'(\xi^i_{N+1}(\tau)) = 0\,, \tag{4.5b}$$

where

$$\mathbf{x}^i(0,\tau) = \mathbf{z}(\xi^i_0(\tau))\,, \tag{4.6a}$$

$$\mathbf{x}^i(1,\tau) = \mathbf{z}(\xi^i_{N+1}(\tau))\,, \tag{4.6b}$$

for some $\xi^i_0(\tau)$ and $\xi^i_{N+1}(\tau)$.

4.1.2 Discretization

The discretization procedure described here is as in [7]. We apply the method of lines, discretizing in space. A staggered grid in σ and second order centered approximations are used. We let $\mathbf{X}_j^i(\tau)$ approximate $\mathbf{x}^i((j-1/2)h,\tau)$ for $j = 0, 1, \ldots, N, N+1$, where h is the grid spacing and $N = 1/h$ is the number of interior grid points. Then to second order we have

$$\mathbf{x}^i(jh) \approx (\mathbf{X}_{j+1}^i + \mathbf{X}_j^i)/2\,. \tag{4.7}$$

The explicit dependence on time will be suppressed for the remainder of this section. Denoting the second order centered approximation of the k^{th} derivative by D_k, we use the following approximations:

$$\mathbf{x}_\sigma^i \approx D_1\mathbf{X}_j^i \equiv (\mathbf{X}_{j+1}^i - \mathbf{X}_{j-1}^i)/2h\,, \tag{4.8}$$

$$\mathbf{x}_{\sigma\sigma}^i \approx D_2\mathbf{X}_j^i \equiv (\mathbf{X}_{j+1}^i - 2\mathbf{X}_j^i + \mathbf{X}_{j-1}^i)/h^2\,. \tag{4.9}$$

We estimate the normal vector, $\hat{\mathbf{n}}_i$, to an interface, Γ_i, by

$$\hat{\mathbf{n}}_i \approx \frac{(D_1\mathbf{X}_j^i)^\perp}{\left|(D_1\mathbf{X}_j^i)\right|}\,. \tag{4.10}$$

The integral in the second term on the right hand side of equation (4.3) is approximated using these discretizations and the trapezoid rule:

$$\kappa_a \equiv \frac{1}{|\Gamma|}\sum_i \int_{\Gamma_i} \frac{\mathbf{x}_{\sigma\sigma}^i}{|\mathbf{x}_\sigma^i|^2}\cdot\hat{\mathbf{n}}_i\,ds \approx \frac{h}{|\Gamma|}\sum_{j=1}^{N}\frac{D_2\mathbf{X}_j^i}{\left|D_1\mathbf{X}_j^i\right|^2}\cdot(D_1\mathbf{X}_j^i)^\perp\,. \tag{4.11}$$

The length of the interfaces is also approximated using a trapezoid scheme:

$$|\Gamma| \approx \sum_i h\sum_{j=1}^{N}\left|D_1\mathbf{X}_j^i\right|\,. \tag{4.12}$$

We use the approximations (4.8), (4.9), (4.10), (4.11), and (4.12), to discretize equation (4.3):

$$\frac{d}{d\tau}\mathbf{X}_j^i = \frac{D_2\mathbf{X}_j^i}{\left|D_1\mathbf{X}_j^i\right|^2} - \kappa_a\frac{(D_1\mathbf{X}_j^i)^\perp}{\left|D_1\mathbf{X}_j^i\right|^2}\,. \tag{4.13}$$

Here κ_a is as given in (4.11). Note that equation (4.13) is independent of h. For closed interfaces, (4.4) requires

$$\mathbf{X}_0^i = \mathbf{X}_N^i\,, \qquad \mathbf{X}_1^i = \mathbf{X}_{N+1}^i\,. \tag{4.14}$$

If an interface is closed, we apply second order forward differencing and averaging to (4.5) and (4.6) to yield the following conditions:

$$(\mathbf{X}_1^i - \mathbf{z}(\xi_0^i)) \cdot \mathbf{z}'(\xi_0^i) = 0\,, \tag{4.15a}$$

$$\mathbf{X}_0^i = 2\mathbf{z}(\xi_0^i) - \mathbf{X}_1^i\,, \tag{4.15b}$$

and

$$(\mathbf{X}_N^i - \mathbf{z}(\xi_{N+1}^i)) \cdot \mathbf{z}'(\xi_{N+1}^i) = 0\,, \tag{4.16a}$$

$$\mathbf{X}_{N+1}^i = 2\mathbf{z}(\xi_{N+1}^i) - \mathbf{X}_N^i\,. \tag{4.16b}$$

Here $\mathbf{z}(\xi_0^i)$ and $\mathbf{z}(\xi_{N+1}^i)$ are unknown points on the boundary curve. These equations can be interpreted geometrically. From (4.15a) and (4.16a) we see that $\mathbf{z}(\xi_0^i)$ and $\mathbf{z}(\xi_{N+1}^i)$ must be the points on the boundary that are closest to $\mathbf{X}_1^i$ and $\mathbf{X}_N^i$ respectively. The points $\mathbf{X}_0^i$ and $\mathbf{X}_{N+1}^i$ are then reflections of $\mathbf{X}_1^i$ and $\mathbf{X}_N^i$ through the closest point on the boundary.

4.1.3 Solving the Discrete Equations Numerically

Given arbitrary initial data, information on whether the curve is closed or intersects the boundary, and a boundary curve, the system of ordinary differential equations, (4.13), and the boundary conditions (4.14) or (4.15) and (4.16), need to be solved in time using some numerical scheme. The code used in this thesis employs the explicit fourth order Runge Kutta method. Other appropriate methods for time stepping are discussed in [7]. For stability, the time steps, k, are chosen to satisfy

$$k = \frac{h^2}{4} \min_{i,j} \left| D_1 \mathbf{X}_j^i \right|^2 . \tag{4.17}$$

If a given interface is closed, then we use (4.14) to ensure that the curve remains closed. We advance equation (4.13) for $j = 0, 1, \ldots, N$ by one time step using the explicit fourth order

Runge Kutta method and values of $\mathbf{X}_j^i$ at the previous time step. This procedure is repeated to advance further in time.

For an interface that intersects the boundary, first we use equations (4.15) and (4.16) to find $\mathbf{X}_0^i$ and $\mathbf{X}_{N+1}^i$ to ensure that the interface intersects the boundary curve orthogonally. We do this using geometrical reasoning for simple boundaries such as circles or squares. For general boundaries parameterized by $\mathbf{z}(\xi)$, we solve (4.15a) and (4.16a) using the bisection method and Newton's method to determine ξ_0^i and ξ_{N+1}^i. We used several iterations of the bisection method to obtain good initial guesses for Newton's method and then Newton's method is repeated until convergence is attained. Equations (4.15b) and (4.16b) are then used to find $\mathbf{X}_0^i$ and $\mathbf{X}_{N+1}^i$. We again use the explicit fourth order Runge Kutta method on (4.13) for $j = 1, 2, \ldots, N$ to advance one time step. We repeat this procedure for subsequent time steps.

The code used in this chapter, based on [7], employs regridding to maintain at least one grid point for every arc length h along an interface curve. *Surgeries* are also done to eliminate curves when they get too short and for other singularities. This is not important for this thesis and the reader is referred to [7] for more information.

4.2 Numerical Results

In this section we examine the evolution of interfaces in several situations using the numerical method described in §4.1. The motion of both closed interfaces and interfaces intersecting the boundary are considered. We make comparisons with analytical results.

4.2.1 Closed Interfaces

We studied the dynamics of a single closed interface using the numerical method. If the initial shape of the interface was convex, the interface would become circular after a while and would remain in this shape for all subsequent time. This agrees with the result stated in the introduction and proven in [9]. See Figure 4.1 for an example of the evolution of a single closed curve. With nonconvex initial conditions, the interface may also become circular as time progresses,

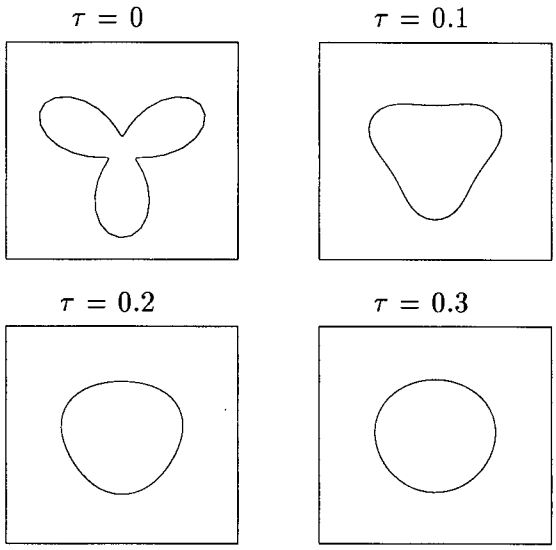

Figure 4.1: Evolution of a closed interface by numerical mean curvature.

but the interface may self-intersect during this evolution. When an interface self-intersects, changes in topology are needed in this case to split the interface into more than one nonintersecting curves. This is not done in this thesis. A different method, such as in [15], is better suited to handle these situations. However, the method used here is more easily applied to considering the motion of curves intersecting a general boundary which is the primary aim of this chapter.

We also examined the evolution of several disjoint closed interfaces. If initial conditions are set so that the interfaces do not self-intersect as time increases, a coarsening process was observed. Each interface becomes circular and then the interfaces enclosing large areas grow while interfaces enclosing small areas shrink. Eventually only one circular interface remains. The evolution of two closed curves is depicted in Figure 4.2. We can estimate the total area enclosed by a closed curve using the trapezoid rule and second order forward differencing and averaging:

$$A_i \approx \sum_{j=1}^{N} (U_{j+1}^i - U_j^i)(V_{j+1}^i + V_j^i)/2\,. \tag{4.18}$$

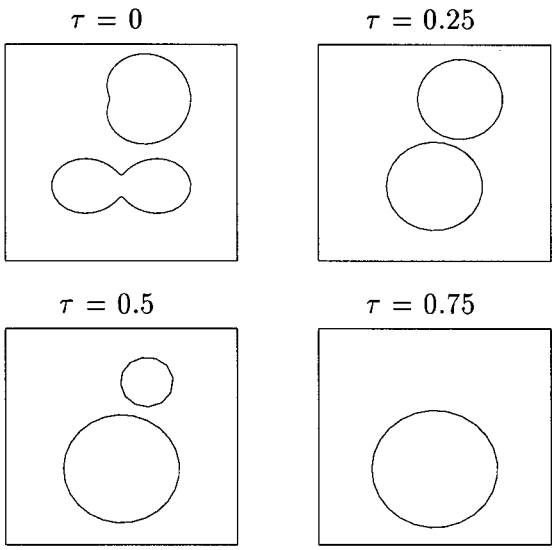

Figure 4.2: Evolution of two closed interfaces by numerical mean curvature.

Here $\mathbf{X}_j^i = (U_j^i, V_j^i)$. Using this we have verified that the total area enclosed by the closed interfaces is approximately constant for one and several interfaces. In fact, aside from the errors associated with the explicit fourth order Runge Kutta method and regridding, the discretization used here preserves discrete area defined by (4.18) [7].

4.2.2 Interfaces Intersecting the Boundary

Boundaries With Constant Curvature

We used the numerical method to track the evolution of interfaces intersecting a boundary that has constant curvature, for example circles and squares. For these two simple boundary curves, Newton's method is not needed to solve (4.15a) and (4.16a). Instead, the closest point on the boundary to the first and last interior grid points can be determined geometrically to ensure that the interfaces intersect the boundary orthogonally. See Figure 4.3 for the evolution of an interface intersecting the unit circle. For the unit circle, we found that interfaces quickly evolve into a smooth convex steady state close to the arc of a circle and the interface does not move

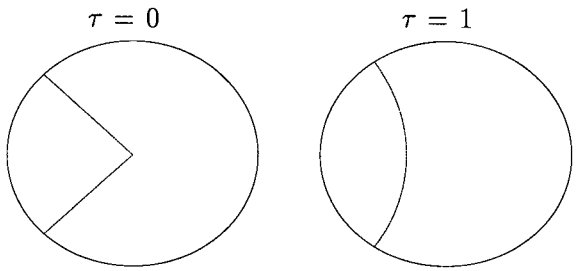

Figure 4.3: Evolution of an interface intersecting the unit circle.

along the boundary. This is as expected since evolution by (1.4) wants to minimize the length of Γ that encloses a specified area [9] and for this boundary, the length of Γ does not change if the contact points with ∂D move along ∂D. This can also be seen explicitly using the asymptotic result for small drops, (4.2) which yields $\xi' = 0$ since $K_D' = 0$ for a circle. When the boundary was a square, the situation is similar.

The convergence of the method is examined for the data used in Figure 4.3 at $\tau = 1$. Since the exact solution is not known, we estimate the error, e_h, by comparing the numerical solution with step size h to the numerical solution on a grid with step size $h/2$. Note that interpolation is needed to compare solutions on different grids since a staggered grid was used. Table 4.1 displays the maximum errors in the euclidean norm and convergence rate of the method. The convergence is second order as expected.

$N = 1/h$	e_h	*rate*
8	0.2091e-2	
16	0.5300e-3	1.98
32	0.1325e-3	2.00
64	0.3336e-4	1.99

Table 4.1: Estimated errors and convergence rates at $\tau = 1$ for initial data of Figure 4.3.

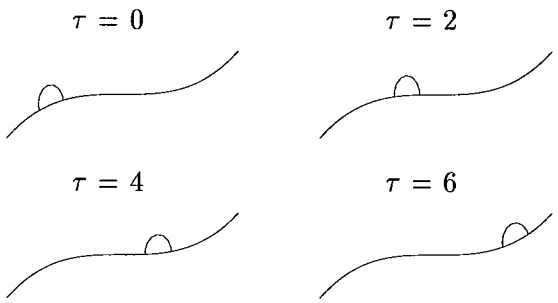

Figure 4.4: Evolution of an interface intersecting the boundary curve $y = x^3$.

Boundaries With Changing Curvature

Next, we examined the evolution of interfaces intersecting boundaries with nonconstant curvature. Given a parameterization of the boundary curve, the bisection method and Newton's method are used to solve (4.15a) and (4.16a) to find the closest points on the boundary to the first and last interior grid points respectively. We found that the interfaces develop into smooth convex shapes intersecting the boundary at right angles, then the interfaces will move along the boundary until a steady state is attained. For small drops, for which the length scale of the drop is small compared to the radius of curvature of the boundary, we observed that the interfaces move along the boundary in the direction of increasing boundary curvature and reach a steady state with the endpoints of the interface surrounding a local maximum of the boundary curvature. See Figures 4.4 and 4.5.

We studied the evolution of an interface intersecting a boundary curve composed of an ellipse with major axis 2 and minor axis 1. This boundary curve, ∂D can be parameterized by

$$\mathbf{z}(\theta) = (2\cos\theta, \sin\theta), \quad 0 \leq \theta \leq 2\pi . \tag{4.19}$$

See Figure 4.5 for the evolution of some initial data intersecting this boundary curve. For this initial data and boundary curve, we found the convergence to be of second order as shown in Table 4.2.

The numerical trajectories of the center of small interfaces intersecting the boundary, or

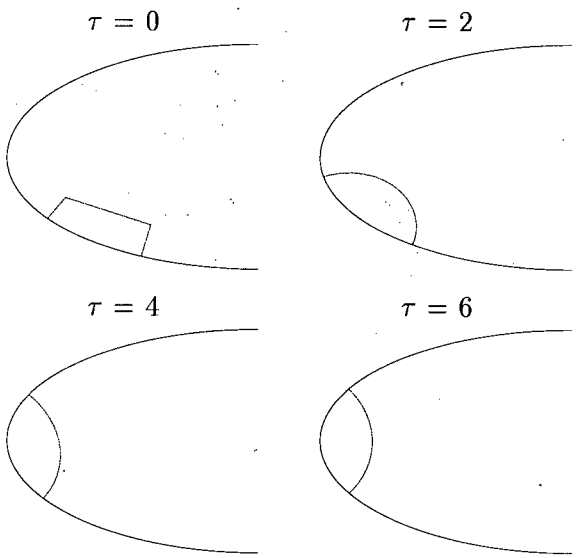

Figure 4.5: Evolution of an interface intersecting an ellipse.

$N = 1/h$	e_h	*rate*
8	0.7214e-1	
16	0.2101e-1	1.78
32	0.5476e-2	1.94
64	0.1407e-2	1.96

Table 4.2: Estimated errors and convergence rates at $\tau = 1$ for initial data of Figure 4.5.

drops, were compared to the asymptotic result (4.2) for several different boundary curves. To do this, we took the location of the center of the drop to be the closest point on the boundary curve to the point midway between the two intersections of the interface with the boundary. We found the boundary parameter, $\theta(\tau)$, for the center using the bisection method and Newton's method. We estimated the area enclosed by the drop and the boundary curve using equation (4.18) and $\mathbf{X}^i_{N+1} = \mathbf{X}^i_0$. The radius of the drop, δ, was estimated by assuming the interface was approximately semi-circular and using the area it enclosed to determine δ. We then track the trajectory of $\theta(\tau)$ in time as the interface evolves under the numerical method. To compare with the asymptotic result, the differential equation, (4.2), is solved numerically using fourth

order Runge Kutta for the given boundary.

For the elliptical boundary curve defined in (4.19), the curvature is given by

$$K_D(\theta) = 2(\sin^2\theta + 4\cos^2\theta)^{-3/2}\,. \tag{4.20}$$

The asymptotic result, (4.2), then becomes

$$\theta'(\tau) = -\frac{24\delta}{\pi}\frac{\sin\theta\cos\theta}{(4\sin^2\theta + \cos^2\theta)^{7/2}}\,. \tag{4.21}$$

We start with the initial data of a small semi-circle centered around the point on ∂D where $\theta(0) = \pi/4$. We observed that these drops move along the boundary in the direction of increasing boundary curvature and a steady state was reached at the local maximum of boundary curvature when $\theta = 0$. The trajectories of $\theta(\tau)$ for the numerical method and the asymptotic differential equation (4.21) are compared for several different drop radii in Figure 4.6. We notice that the numerical trajectory gets closer to the asymptotic trajectory as δ is decreased. For very small radii, both trajectories are very similar.

We also considered boundary curves of the following form [11]:

$$\mathbf{z}(\theta) = (p(\theta)\cos\theta - p'(\theta)\sin\theta, p(\theta)\sin\theta + p'(\theta)\cos\theta)\,, \quad 0 \le \theta \le 2\pi\,. \tag{4.22}$$

Given any $p(\theta)$ such that $p(\theta) = p(\theta + 2\pi)$, $p(\theta) > 0$, and $p(\theta) + p''(\theta) > 0$, (4.22) generates a strictly convex domain. The curvature of such a domain is given by

$$K_D(\theta) = [p(\theta) + p''(\theta)]^{-1}\,. \tag{4.23}$$

For these boundary curves, the asymptotic differential equation for the center of a drop, (4.2), becomes

$$\theta'(\tau) = -\frac{4\delta}{3\pi}\frac{(p'(\theta) + p'''(\theta))}{(p(\theta) + p''(\theta))^4}\,. \tag{4.24}$$

We examined the numerical evolution of small interfaces intersecting ∂D for the following two forms of $p(\theta)$:

$$p = p_1(\theta) \equiv 3 + 0.4\sin^3\theta - 0.5\cos^2\theta\,, \tag{4.25}$$

$$p = p_2(\theta) \equiv 3 + 1.4\sin^3\theta\,. \tag{4.26}$$

These domains are plotted in Figure 4.7 and Figure 4.8. We started with the initial data of a small semi-circle centered around the point on ∂D for which $\theta(0) = \pi/3$. The location of the center of the drop and the radius are determined as for the elliptical boundary. Trajectories of $\theta(\tau)$ for the numerical method and for the asymptotic result, (4.24), are displayed in Figure 4.9 and Figure 4.10. Referring to Figures 4.6, 4.9, and 4.10, we see that the motion by numerical area preserving mean curvature is very similar to the asymptotic result for motion of small drops along a boundary curve, (4.2), as $\delta \to 0$. Thus the results in this chapter numerically verify (4.2).

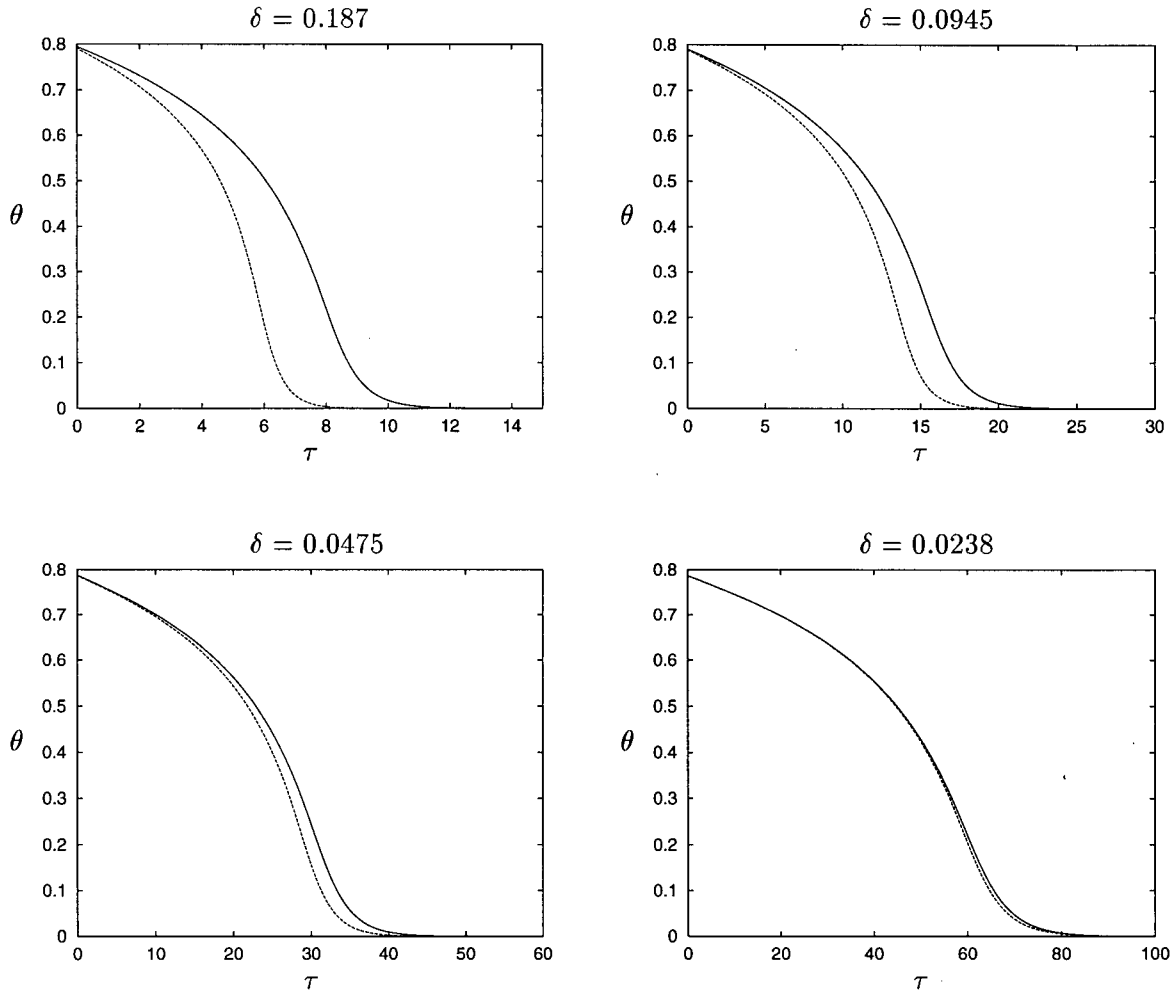

Figure 4.6: Plots of θ vs time for different δ. The boundary curve is the ellipse defined in (4.19). The solid lines are the asymptotic result given by (4.21) and the dashed lines are the result from numerical motion by curvature.

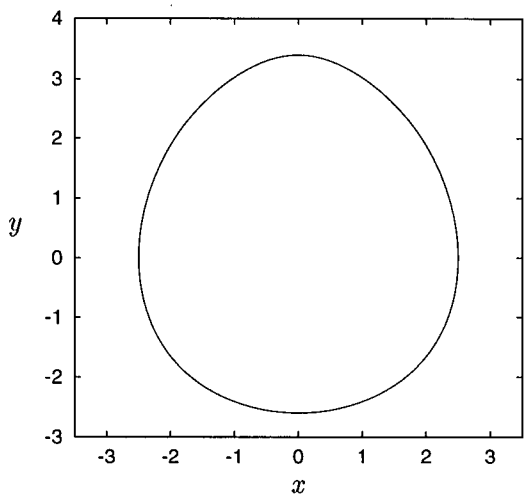

Figure 4.7: The domain with boundary given by (4.22) with $p = p_1(\theta) \equiv 3+0.4\sin^3\theta-0.5\cos^2\theta$.

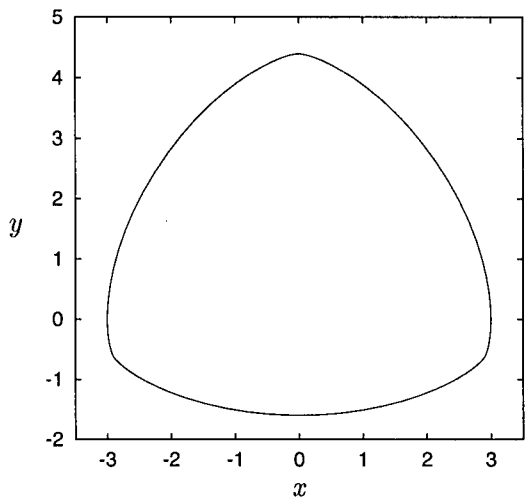

Figure 4.8: The domain with boundary given by (4.22) with $p = p_2(\theta) \equiv 3 + 1.4\sin^3\theta$.

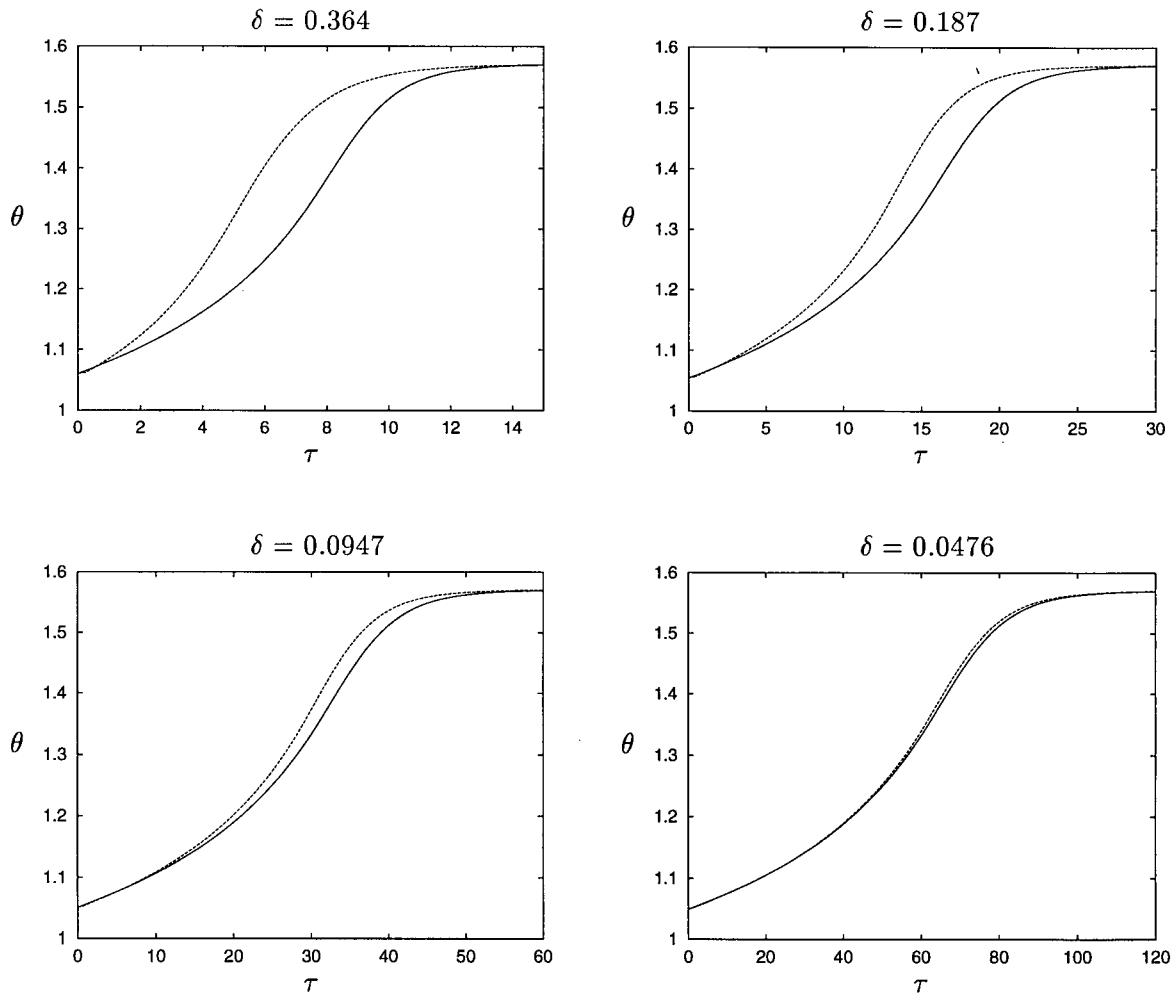

Figure 4.9: Plots of θ vs time for different δ. Here ∂D is parameterized by $p = p_1(\theta) \equiv 3 + 0.4\sin^3\theta - 0.5\cos^2\theta$. The solid lines are the asymptotic result given by (4.24) and the dashed lines are the result from numerical motion by curvature.

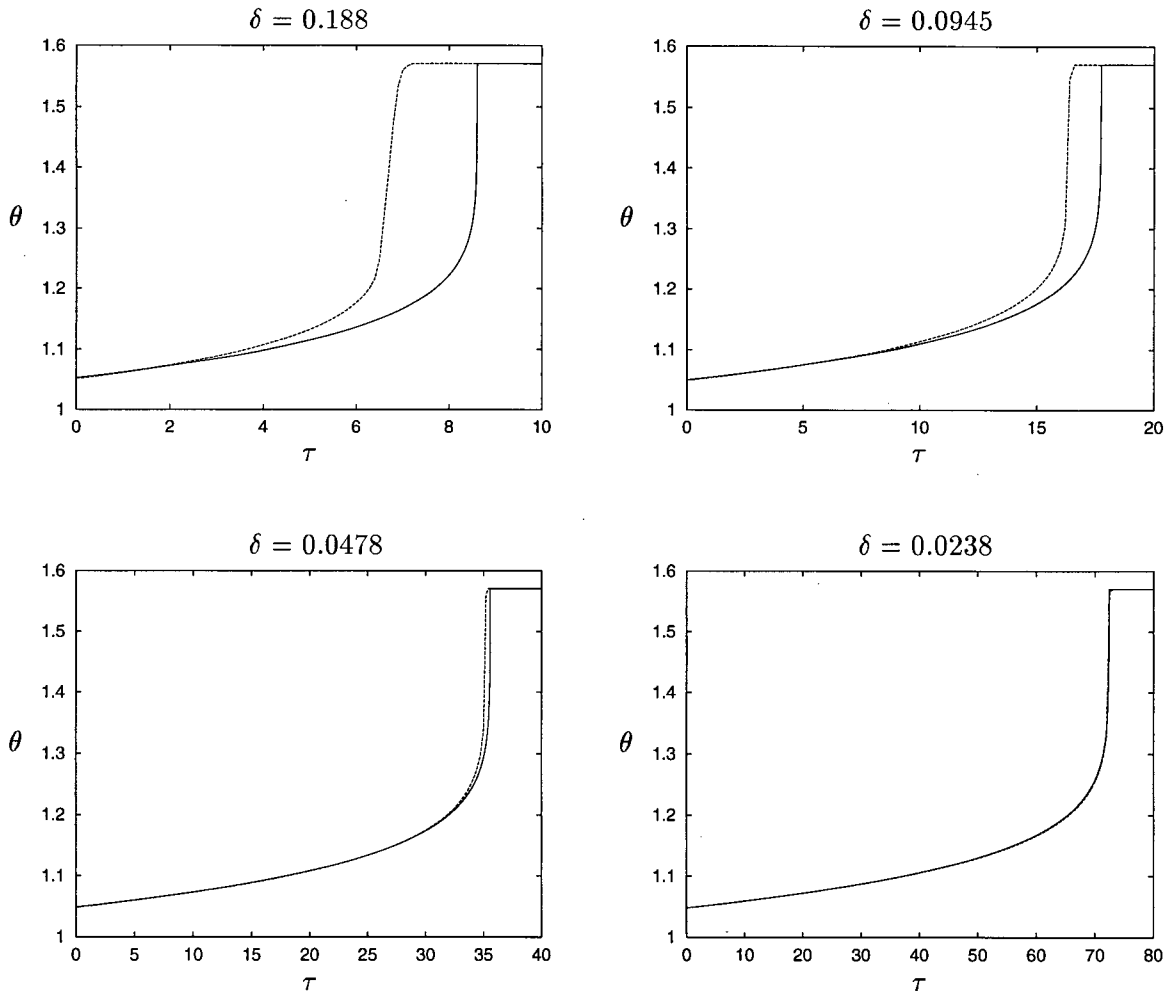

Figure 4.10: Plots of θ vs time for different δ. Here ∂D is parameterized by $p = p_2(\theta) \equiv 3 + 1.4\sin^3\theta$. The solid lines are the asymptotic result given by (4.24) and the dashed lines are the result from numerical motion by curvature.

Chapter 5

Metastable Motion In The Unconstrained Allen-Cahn Equation

A model for phase separation of a binary mixture without a mass constraint is the (unconstrained) Allen-Cahn equation [14]:

$$u_t = \epsilon^2 \Delta u + Q(u), \qquad \mathbf{x} \in D \subset \mathbf{R^2}, \tag{5.1a}$$

$$\partial_n u = 0, \qquad \mathbf{x} \in \partial D. \tag{5.1b}$$

In the above, $\mathbf{x} = (x, y)$, $\epsilon \ll 1$, D is a bounded two-dimensional domain, and $Q(u)$ has three zeroes located at $u = s_- < 0$, $u = 0$, and $u = s_+ > 0$. In addition $Q(u)$ satisfies

$$Q(s_\pm) < 0, \quad Q(0) > 0, \quad V(s_+) = 0, \quad V(u) = -\int_{s_-}^{u} Q(\eta)\, d\eta. \tag{5.2}$$

As for the constrained Allen-Cahn equation, the method of matched asymptotic expansion can be used to show that, given initial data, the solution to (5.1) will quickly evolve into regions where $u \sim s_+$ and $u \sim s_-$ with internal layers of width $O(\epsilon)$ separating these two phases. For the Allen-Cahn equation, the normal velocity, v, of such an internal layer, also called an interface, is governed to leading order by (see [14])

$$v \sim \epsilon^2 \kappa. \tag{5.3}$$

Here κ is the mean curvature of the interface. This is referred to as motion by mean curvature. If an interface intersects the boundary of the domain, ∂D, then it must do so orthogonally.

In this chapter, we describe the dynamics of (5.1) when (5.3) fails to give any information about the motion of an interface. This happens when the interface is a straight line as then $\kappa = 0$. A scenario in which this can happen is examined. The goal then is to calculate further terms in the expansion of the interface velocity. The 2-dimensional domain, D, is taken be

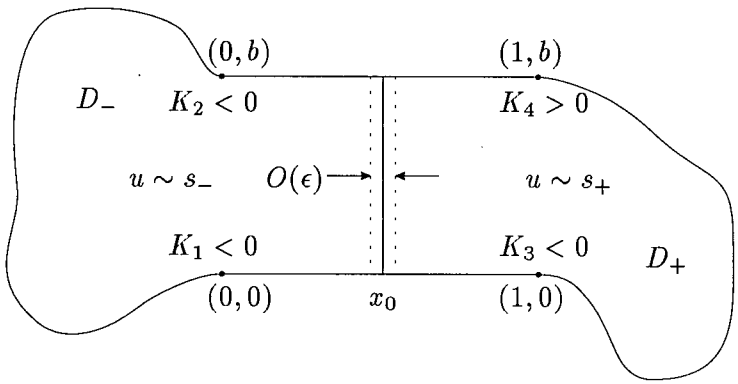

Figure 5.1: Plot of a typical domain D and an interface located at x_0.

$D = R \cup D_- \cup D_+$ where R is the rectangle $[0,1] \times [0,b]$, and D_- and D_+ are two attachments on its sides (see Figure 5.1). From initial data, the solution to (5.1) is assumed to have developed a single vertical straight line interface located at $x = x_0$ with $0 < x_0 < 1$. Notice that there are an infinite number of such solutions that are equilibria for (5.3).

The points $(0,0)$, $(0,b)$, $(1,0)$, and $(1,b)$ are referred to as the corners of R. It is assumed that the domain boundary is smooth and that near the corners of the rectangle, ∂D can be represented as the graph of a function. That is, near each corner, $\partial D = \{(x,y) \,|\, y = \psi_i(x)\}$ where

$$\text{near } (0,0), \quad y = \psi_1(x), \tag{5.4a}$$

$$\text{near } (0,b), \quad y = \psi_2(x) + b, \tag{5.4b}$$

$$\text{near } (1,0), \quad y = \psi_3(x), \tag{5.4c}$$

$$\text{near } (1,b), \quad y = \psi_4(x) + b. \tag{5.4d}$$

It is assumed that there exist numbers $K_i \neq 0$, $\alpha_i > 1$, for $i = 1, \ldots, 4$ such that

$$\psi_1'(x) \sim -K_1(-x)^{\alpha_1}, \quad \text{as } x \to 0^-, \tag{5.5a}$$

$$\psi_2'(x) \sim K_2(-x)^{\alpha_2}, \quad \text{as } x \to 0^-, \tag{5.5b}$$

$$\psi_3'(x) \sim K_3(x-1)^{\alpha_3}, \quad \text{as } x \to 1^+, \tag{5.5c}$$

$$\psi_4'(x) \sim -K_4(x-1)^{\alpha_4}, \quad \text{as } x \to 1^+. \tag{5.5d}$$

When $\alpha_i = 2$, the constant K_i is proportional to the curvature of the i^{th} corner.

In this situation the conventional method of matched asymptotics fails to determine the motion of the straight line interfaces. Instead, the projection method, [17], [18], is used to calculate the dynamics. First, an equilibrium solution to (5.1) in R is constructed. Next, the spectral properties obtained by linearizing (5.1) around the equilibrium solution are analyzed asymptotically. The principal eigenvalue is found to be exponentially small, so metastable motion is expected. Finally, this information is combined with the projection method to derive an explicit ODE for the motion of the interface location.

5.1 The Equilibrium Solution

In the limit $\epsilon \to 0$, an equilibrium solution to (5.1) in the rectangle, R, is found. We assume that this solution is only a function of x and has exactly one internal layer centered at $x = x_0$, $0 < x_0 < 1$. Denoting this equilibrium solution as $U_b(z)$ where $z = \epsilon^{-1}(x - x_0)$, it satisfies

$$U_b'' + Q(U_b) = 0, \quad -\infty < z < \infty, \tag{5.6a}$$

$$U_b(0) = 0; \quad U_b(z) \sim s_\pm, \quad \text{as } z \to \pm\infty. \tag{5.6b}$$

Thus, asymptotically $U_b(z)$ is given by

$$U_b(z) \sim \begin{cases} s_+ - a_+ e^{-\nu_+ z}, & z \to +\infty\,, \\ s_- + a_- e^{\nu_- z}, & z \to -\infty\,. \end{cases} \tag{5.7}$$

Here the positive constants $\nu_\pm$ and $a_\pm$ are defined by

$$\nu_\pm = \left[-Q'(s_\pm)\right]^{1/2}, \tag{5.8}$$

$$\log a_\pm = \log(\pm s_\pm) + \int_0^{s_\pm} \left(\frac{\pm\nu_\pm}{[2V(\eta)]^{1/2}} + \frac{1}{\eta - s_\pm} \right) d\eta\,. \tag{5.9}$$

5.2 Spectral Estimates for the Linearized Problem

The eigenvalue problem associated with linearizing (5.1) about the equilibrium solution $U_b[\epsilon^{-1}(x-x_0)]$ is

$$L_\epsilon\phi \equiv \epsilon^2\Delta\phi + Q'(U_b)\phi = \lambda\phi\,, \qquad \mathbf{x}\in D\,, \tag{5.10a}$$

$$\partial_n\phi = 0\,, \qquad \mathbf{x}\in\partial D\,, \tag{5.10b}$$

$$(\phi,\phi) = \int_D \phi^2\,d\mathbf{x}\,. \tag{5.10c}$$

Here $(u,v)\equiv\int_D uv\,d\mathbf{x}$. The eigenvalues and eigenfunction of (5.10) are labeled by λ_j and ϕ_j respectively for $j=0,1,\ldots$, with $\lambda_j\to-\infty$ as $j\to\infty$.

To estimate the principal eigenpair it is assumed that the distance from the interface to the corners of R is $O(1)$. Notice that $L_\epsilon U_b'[\epsilon^{-1}(x-x_0)] = 0$. Then from (5.7), $U_b'[\epsilon^{-1}(x-x_0)]$ fails to satisfy the boundary condition (5.10b) by only exponentially small terms. Thus, $\phi_0\sim N_0\,[U_b'+\phi_{L_0}]$ where N_0 is a normalization constant and ϕ_{L_0} is a boundary layer function localized near the curved parts of ∂D that is used to satisfy the boundary condition (5.10b). Green's identity can be applied to (5.10a) and U_b' to estimate the principal eigenvalue:

$$\lambda_0(U_b',\phi_0) = -\epsilon^2\int_{\partial D}\phi_0\partial_n U_b'\,ds\,. \tag{5.11}$$

To calculate ϕ_{L_0}, a local coordinate system defined near ∂D is used. We set $\eta = n/\epsilon$, where $-n$ is the distance from $\mathbf{x}\in D$ to ∂D, and let ξ be a coordinate perpendicular to n. Then, when $\eta=O(1)$ and $x<x_0$, $U_b\sim s_-$ so (5.10) gives

$$\begin{gathered}\partial_{\eta\eta}\phi_{L_0} - \nu_-^2\phi_{L_0} = 0\,, \quad \eta<0\,; \quad \phi_{L_0}\to 0\,, \text{ as } \eta\to-\infty\,,\\ \partial_\eta\phi_{L_0}|_{\eta=0} = -\epsilon\partial_n U_b'|_{\eta=0}\,.\end{gathered} \tag{5.12}$$

Similarly, when $\eta=O(1)$ and $x>x_0$, $U_b\sim s_+$ and so we get

$$\begin{gathered}\partial_{\eta\eta}\phi_{L_0} - \nu_+^2\phi_{L_0} = 0\,, \quad \eta<0\,; \quad \phi_{L_0}\to 0\,, \text{ as } \eta\to-\infty\,,\\ \partial_\eta\phi_{L_0}|_{\eta=0} = -\epsilon\partial_n U_b'|_{\eta=0}\,.\end{gathered} \tag{5.13}$$

Solving these equations we get

$$\phi_{L_0} = \begin{cases} [-\epsilon\partial_n U_b'] \,|_{\eta=0} e^{\nu_- \eta} & x < x_0\,, \\ [-\epsilon\partial_n U_b'] \,|_{\eta=0} e^{\nu_+ \eta} & x > x_0\,. \end{cases} \tag{5.14}$$

Using (5.7), we obtain that

$$U_b' \sim \begin{cases} a_-\nu_- e^{\nu_- \epsilon^{-1}(x-x_0)} & x < x_0\,, \\ a_+\nu_+ e^{-\nu_+ \epsilon^{-1}(x-x_0)} & x > x_0\,, \end{cases} \tag{5.15}$$

and

$$\partial_n U_b' \sim \begin{cases} a_-\nu_-^2 \epsilon^{-1} e^{\nu_- \epsilon^{-1}(x-x_0)} n_x & x < x_0\,, \\ -a_+\nu_+^2 \epsilon^{-1} e^{-\nu_+ \epsilon^{-1}(x-x_0)} n_x & x > x_0\,. \end{cases} \tag{5.16}$$

Here $\hat{\mathbf{n}} = (n_x, n_y)$ is the outward unit normal vector to ∂D. Substituting (5.16) into (5.14) and using (5.14) and (5.15) in $\phi_0 \sim N_0 [U_b' + \phi_{L_0}]$ we get

$$\phi_0 \sim \begin{cases} N_0 a_-\nu_- e^{\nu_- \epsilon^{-1}(x-x_0)} \left(1 - \nu_- n_x e^{\nu_- \epsilon^{-1}\eta}\right) & x < x_0\,, \\ N_0 a_+\nu_+ e^{-\nu_+ \epsilon^{-1}(x-x_0)} \left(1 + \nu_+ n_x e^{\nu_+ \epsilon^{-1}\eta}\right) & x > x_0\,. \end{cases} \tag{5.17}$$

So on ∂D, ϕ_0 is given by

$$\phi_0 \sim \begin{cases} N_0 a_-\nu_- e^{\nu_- \epsilon^{-1}(x-x_0)} (1 - \nu_- n_x) & x < x_0\,, \\ N_0 a_+\nu_+ e^{-\nu_+ \epsilon^{-1}(x-x_0)} (1 + \nu_+ n_x) & x > x_0\,. \end{cases} \tag{5.18}$$

To estimate N_0 and λ_0, (U_b', U_b') needs to be evaluated. This is done using a Laplace type argument as U_b' is localized near $x = x_0$. This yields

$$(U_b', U_b') \sim \int_0^b \int_{-\infty}^{\infty} \epsilon \left[U_b'(z)\right]^2 \, dz \, dy \sim \epsilon b \beta\,, \tag{5.19}$$

where

$$\beta \equiv \int_{-\infty}^{\infty} \left[U_b'(z)\right]^2 \, dz\,. \tag{5.20}$$

Since $\phi_0 \sim N_0 U_b'$, the normalization constant, N_0, satisfies

$$N_0 \sim (\epsilon b \beta)^{-1/2}\,. \tag{5.21}$$

To evaluate the right side of (5.11) we notice from (5.16) that $\partial_n U_b' = 0$ except along the two attachments to the rectangle, D_+ and D_-, since $n_x = 0$ on R. Using this and substituting (5.16), (5.18), and (5.19) into (5.11), we obtain the following asymptotic estimate for λ_0:

$$\lambda_0 \sim \frac{1}{b\beta}\{I_2 - I_1\}\,. \tag{5.22}$$

In equation (5.22), I_1 and I_2 are given by

$$I_1 = \int_{\partial D_-} a_-^2 \nu_-^3 e^{2\nu_- \epsilon^{-1}(x-x_0)}(1-\nu_- n_x) n_x \, ds\,, \tag{5.23}$$

$$I_2 = \int_{\partial D_+} a_+^2 \nu_+^3 e^{-2\nu_+ \epsilon^{-1}(x-x_0)}(1+\nu_+ n_x) n_x \, ds\,. \tag{5.24}$$

Here ∂D_- and ∂D_+ are traversed in the counterclockwise direction. Near the corners, the x component of the outward normal vectors to D can be calculated from (5.5) to yield

$$n_x = \frac{-K_1(-x)^{\alpha_1}}{\left[K_1^2(-x)^{2\alpha_1}+1\right]^{1/2}} \quad \text{near } (0,0) \text{ as } x \to 0^-\,, \tag{5.25a}$$

$$n_x = \frac{-K_2(-x)^{\alpha_2}}{\left[K_2^2(-x)^{2\alpha_2}+1\right]^{1/2}} \quad \text{near } (0,b) \text{ as } x \to 0^-\,, \tag{5.25b}$$

$$n_x = \frac{K_3(x-1)^{\alpha_3}}{\left[K_3^2(x-1)^{2\alpha_3}+1\right]^{1/2}} \quad \text{near } (1,0) \text{ as } x \to 1^+\,, \tag{5.25c}$$

$$n_x = \frac{K_4(x-1)^{\alpha_4}}{\left[K_4^2(x-1)^{2\alpha_4}+1\right]^{1/2}} \quad \text{near } (1,b) \text{ as } x \to 1^+\,. \tag{5.25d}$$

Because the integrands in (5.23) and (5.24) are exponentially decreasing away from the location of the interface, $x = x_0$, the dominant contribution to these integrals arises from $O(\epsilon)$ regions near the corners. In these regions, $n_x \gg n_x^2$, so I_1 and I_2 can be estimated using (5.25) and Laplace's method as follows:

$$I_1 \sim a_-^2 \nu_-^3 \left[K_1 \int_0^{-\infty} (-x)^{\alpha_1} e^{2\nu_- \epsilon^{-1}(x-x_0)}\,dx + K_2 \int_0^{-\infty} (-x)^{\alpha_2} e^{2\nu_- \epsilon^{-1}(x-x_0)}\,dx\right]\,, \tag{5.26}$$

$$I_2 \sim a_+^2 \nu_+^3 \left[K_3 \int_1^{\infty} (x-1)^{\alpha_3} e^{-2\nu_+ \epsilon^{-1}(x-x_0)}\,dx + K_4 \int_1^{\infty} (x-1)^{\alpha_4} e^{-2\nu_+ \epsilon^{-1}(x-x_0)}\,dx\right]\,. \tag{5.27}$$

These integrals can be evaluated to obtain

$$I_1 \sim -a_-^2 \nu_-^3 \left[K_1 \left(\frac{\epsilon}{2\nu_-}\right)^{\alpha_1+1} \Gamma(\alpha_1+1) + K_2 \left(\frac{\epsilon}{2\nu_-}\right)^{\alpha_2+1} \Gamma(\alpha_2+1)\right] e^{-2\nu_- \epsilon^{-1} x_0}\,, \tag{5.28}$$

$$I_2 \sim a_+^2 \nu_+^3 \left[K_3 \left(\frac{\epsilon}{2\nu_+}\right)^{\alpha_3+1} \Gamma(\alpha_3+1) + K_4 \left(\frac{\epsilon}{2\nu_+}\right)^{\alpha_4+1} \Gamma(\alpha_4+1)\right] e^{-2\nu_+ \epsilon^{-1}(1-x_0)}\,. \tag{5.29}$$

Therefore, the principal eigenvalue, λ_0, is exponentially small and is given asymptotically by

$$\lambda_0 \sim \frac{1}{b\beta}\left\{a_-^2\nu_-^3\left[K_1\left(\frac{\epsilon}{2\nu_-}\right)^{\alpha_1+1}\Gamma(\alpha_1+1)+K_2\left(\frac{\epsilon}{2\nu_-}\right)^{\alpha_2+1}\Gamma(\alpha_2+1)\right]e^{-2\nu_-\epsilon^{-1}x_0}\right.$$
$$\left. + \; a_+^2\nu_+^3\left[K_3\left(\frac{\epsilon}{2\nu_+}\right)^{\alpha_3+1}\Gamma(\alpha_3+1)+K_4\left(\frac{\epsilon}{2\nu_+}\right)^{\alpha_4+1}\Gamma(\alpha_4+1)\right]e^{-2\nu_+\epsilon^{-1}(1-x_0)}\right\}. \quad (5.30)$$

5.3 The Projection Method

The projection method is now applied to determine the trajectory of the interface location, $x_0 = x_0(t)$, for the time dependent problem, (5.1), in the domain D. It is assumed that the initial data is an equilibrium solution $u(\mathbf{x},0) = U_b[\epsilon^{-1}(x - x_0^0)]$ with $x_0(0) = x_0^0$. We set $u(\mathbf{x},t) = U_b[\epsilon^{-1}(x - x_0(t))] + w(\mathbf{x},t)$. It is assumed that $w \ll U_b$ and $w_t \ll \partial_t U_b$ uniformly in time. Using this, we linearize (5.1) about U_b to produce

$$L_\epsilon w \equiv \epsilon^2\Delta w + Q'(U_b)w = \partial_t U_b\,, \qquad \mathbf{x}\in D\,, \quad (5.31a)$$

$$\partial_n w = -\partial_n U_b, \qquad \mathbf{x}\in \partial D\,. \quad (5.31b)$$

The solution to (5.31) is expanded in terms of the eigenfunctions of (5.10) as $w = \sum_{j=0}^{\infty} c_j\phi_j/\lambda_j$. Integrating by parts, we get

$$(\phi_j, L_\epsilon w) - (w, L_\epsilon\phi_j) = (\phi_j, \partial_t U_b) - \lambda_j(w,\phi_j)\,. \quad (5.32)$$

Next, using Green's identity and $\lambda_j(w,\phi_j) = c_j$ in (5.32), it is found that the coefficients c_j for $j = 0, 1, \ldots$, satisfy

$$c_j = (\phi_j, \partial_t U_b) + \epsilon^2\int_{\partial D}\phi_j\partial_n U_b\, ds\,. \quad (5.33)$$

Since λ_0, as estimated in (5.30), is exponentially small, to ensure that $w \ll U_b$ over exponentially long time intervals it is required that $c_0 = 0$. Then (5.33) produces the slow motion equation:

$$(\phi_0, \partial_t U_b) = -\epsilon^2\int_{\partial D}\phi_0\partial_n U_b\, ds\,. \quad (5.34)$$

Next the terms in (5.34) are evaluated to determine the motion of the interface. To calculate $(\phi_0, \partial_t U_b)$, we substitute $\partial_t U_b = -\epsilon^{-1}x_0'(t)U_b'$ in (5.34) and use the result of (5.19) to obtain

$$(\phi_0, \partial_t U_b) \sim -b\beta x_0'(t)\,. \quad (5.35)$$

To evaluate the right side of (5.34), (5.7) is used to determine that

$$\partial_n U_b \sim \begin{cases} a_-\nu_-\epsilon^{-1}e^{\nu_-\epsilon^{-1}(x-x_0)}n_x & x < x_0\,, \\ a_+\nu_+\epsilon^{-1}e^{-\nu_+\epsilon^{-1}(x-x_0)}n_x & x > x_0\,. \end{cases} \tag{5.36}$$

Thus, an argument similar to that used to derive (5.22) produces

$$\epsilon^2 \int_{\partial D} \phi_0 \partial_n U_b \, ds \sim \epsilon\nu_-^{-1} I_1 + \epsilon\nu_+^{-1} I_2\,, \tag{5.37}$$

where I_1 and I_2 are defined in (5.23) and (5.24) respectively. Combining the results of (5.28), (5.29), (5.35), and (5.37) determines the differential equation governing the slow motion of the interface:

$$\begin{aligned} x_0'(t) \;\sim\; & \frac{\epsilon}{b\beta}\left\{ a_+^2\nu_+^2\left[K_3\left(\frac{\epsilon}{2\nu_+}\right)^{\alpha_3+1}\Gamma(\alpha_3+1) + K_4\left(\frac{\epsilon}{2\nu_+}\right)^{\alpha_4+1}\Gamma(\alpha_4+1)\right]e^{-2\nu_+\epsilon^{-1}(1-x_0)}\right. \\ & \left. - a_-^2\nu_-^2\left[K_1\left(\frac{\epsilon}{2\nu_-}\right)^{\alpha_1+1}\Gamma(\alpha_1+1) + K_2\left(\frac{\epsilon}{2\nu_-}\right)^{\alpha_2+1}\Gamma(\alpha_2+1)\right]e^{-2\nu_-\epsilon^{-1}x_0}\right\}. \end{aligned} \tag{5.38}$$

It is seen that the motion of the interface location is determined by the shape of the boundary at the corners of the rectangle and the distance from the interface to these corners. The interface will move according to (5.38) until a steady state is attained or until the interface has moved to one of the sides of R. In the latter case, the subsequent evolution of the interface is determined by (5.3). This result agrees with [3] and [12] obtained using a different method.

5.4 Steady States

Steady state locations for the interface can be determined from (5.38). Labelling

$$A_- = K_1\left(\frac{\epsilon}{2\nu_-}\right)^{\alpha_1+1}\Gamma(\alpha_1+1) + K_2\left(\frac{\epsilon}{2\nu_-}\right)^{\alpha_2+1}\Gamma(\alpha_2+1)\,, \tag{5.39a}$$

$$A_+ = K_3\left(\frac{\epsilon}{2\nu_+}\right)^{\alpha_3+1}\Gamma(\alpha_3+1) + K_4\left(\frac{\epsilon}{2\nu_+}\right)^{\alpha_4+1}\Gamma(\alpha_4+1)\,, \tag{5.39b}$$

a steady state exists when $A_-A_+ > 0$. The unique equilibrium interface location is given by

$$x_0^e \sim \frac{\nu_+}{\nu_+ + \nu_-} + \frac{\epsilon}{2(\nu_+ + \nu_-)}\log\left(\frac{a_-^2\nu_-^2 A_-}{a_+^2\nu_+^2 A_+}\right). \tag{5.40}$$

This equilibrium solution is asymptotically stable when $A_- < 0$ and $A_+ < 0$. If $K_i < 0$ for $i = 1, \ldots, 4$, then this corresponds to a domain that is nonconvex near the corners. (See Figure 5.3.) When $A_- > 0$ and $A_+ > 0$, then the equilibrium is unstable. A sufficient condition for this is that $K_i > 0$ for $i = 1, \ldots, 4$. This corresponds to the case of a domain that is convex near the corners. When a steady state exists we note that it is located an $O(\epsilon)$ distance from $\frac{\nu_+}{\nu_+ + \nu_-}$.

5.5 Examples of Slow Dynamics

The following form was considered for $Q(u)$:

$$Q(u) = 2(u - u^3)\,. \tag{5.41}$$

In this case, from (5.6), the equilibrium solution, $U_b(z)$, is given by

$$U_b(z) = \tanh z\,. \tag{5.42}$$

In addition, using (5.8), (5.9), and (5.20), the constants $\nu_\pm$, $a_\pm$, $s_\pm$, and β are found to be

$$\nu_\pm = 2\,, \quad a_\pm = 2\,, \quad s_\pm = \pm 1\,, \quad \beta = 4/3\,. \tag{5.43}$$

For this example, we suppose that $\alpha_1 = \alpha_2 = \alpha_3 = \alpha_4 = \alpha$. Then the ODE for the interface location, (5.38), is

$$x_0' \sim \frac{12\epsilon^{\alpha+2}\Gamma(\alpha+1)}{b4^{\alpha+1}} \left[(K_3 + K_4)e^{-4\epsilon^{-1}(1-x_0)} - (K_1 + K_2)e^{-4\epsilon^{-1}x_0}\right]\,. \tag{5.44}$$

The steady state interface location, (5.40), becomes

$$x_0^e \sim \frac{1}{2} + \frac{\epsilon}{8}\log\left(\frac{K_1 + K_2}{K_3 + K_4}\right)\,. \tag{5.45}$$

If $K_i < 0$ for $i = 1, \ldots, 4$, then this steady state is stable. See Figure 5.2 for an example of such a domain. If $K_i > 0$ for $i = 1, \ldots, 4$, then the steady state is unstable.

Notice that when K_1, $K_2 < 0$ and K_3, $K_4 > 0$, then from (5.44), $x_0' > 0$ for all time. In this case, the interface location, x_0 will monotonically approach 1. See Figure 5.3 for an example of

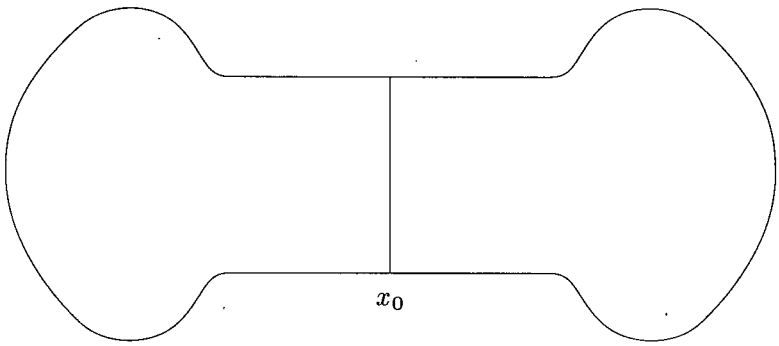

Figure 5.2: Plot of a domain, D, that exhibits a stable steady state interface location. $K_i < 0$ for $i = 1, \ldots, 4$, in this domain and for the parameter values in §5.5, the steady state interface location, x_0^e is given by (5.45).

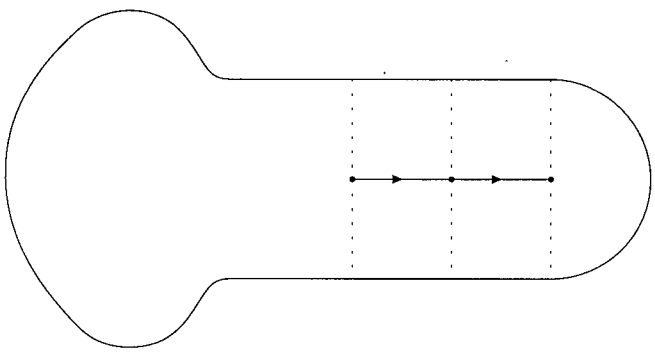

Figure 5.3: Plot of a domain, D, in which the interface moves toward the right. K_1, $K_2 < 0$ and K_3, $K_4 > 0$ for this domain.

such a domain. For the domain in Figure 5.3, the interface will move according to (5.44) until it reaches $x_0 = 1$. Then the interface dynamics will be determined by (5.3) and the interface will eventually disappear against the right side boundary of D. Similarly, when K_1, $K_2 > 0$, and K_3, $K_4 < 0$, $x_0' < 0$ and the interface location will monotonically approach 0.

Chapter 6

Metastable Motion Along ∂D In The Constrained Allen-Cahn Equation

The Allen-Cahn equation with a mass constraint is:

$$u_t = \epsilon^2 \Delta u + Q(u) - \sigma\,, \qquad \mathbf{x} \in D \subset \mathbf{R^2}\,, \tag{6.1a}$$

$$\partial_n u = 0\,, \qquad \mathbf{x} \in \partial D\,, \tag{6.1b}$$

$$\int_D u(\mathbf{x},t)\,d\mathbf{x} = M\,. \tag{6.1c}$$

Here $\mathbf{x} = (x,y)$, $\epsilon \ll 1$, D is a bounded two-dimensional domain, and $Q(u)$ has three zeroes located at $u = s_- < 0$, $u = 0$, and $u = s_+ > 0$. As in earlier chapters, $Q(u)$ is taken to satisfy

$$Q(s_\pm) < 0\,, \quad Q(0) > 0\,, \quad V(s_+) = 0\,, \quad V(u) = -\int_{s_-}^{u} Q(\eta)\,d\eta. \tag{6.2}$$

Recall from Chapter 2 that the solution to (6.1) quickly develops interfaces that evolve to leading order by

$$v \sim \epsilon^2 \left(\kappa - \frac{1}{|\Gamma|}\int_\Gamma \kappa\,ds\right)\,, \tag{6.3}$$

where v is the normal velocity of an interface, Γ. Here κ is the curvature of Γ.

For an interface where κ is a constant, (6.3) yields $v = 0$ and hence it gives no indication of the nature of the motion of such an interface. This happens when the interface is a circle lying completely inside the domain, or when the interface is an arc of a circle intersecting the boundary at right angles. Metastable motion for the case of a circular interface inside a domain was examined in [18] using the projection method. In this chapter, the case of a semi-circular interface intersecting a flat boundary is studied. The following situation is considered. The two-dimensional domain, D, is taken to have a smooth boundary which has a straight-line segment between $(x_L, 0)$ and $(x_R, 0)$ (see Figure 6.1). The solution to (6.1) is assumed to have

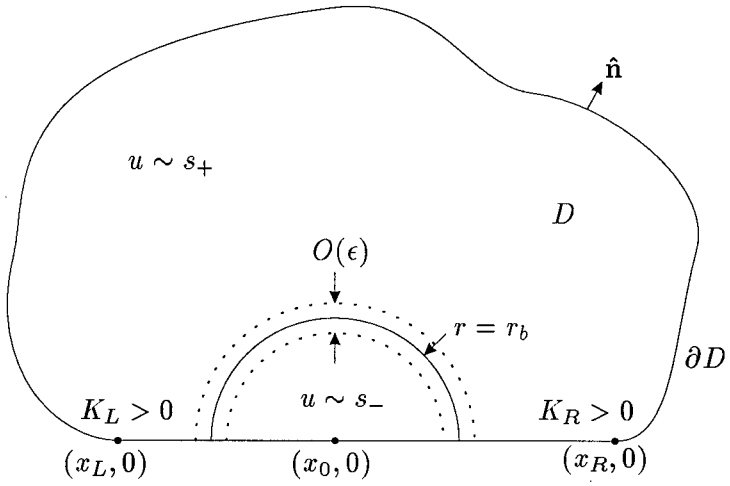

Figure 6.1: Plot of a two-dimensional domain D with a flat boundary segment and a semi-circular interface of radius $r = r_b$ centered at x_0.

developed a single semi-circular interface of radius $r = r_b$ that intersects the boundary of D on this straight-line segment. This interface is taken to be centered around $\mathbf{x}_0 = (x_0, 0)$ where $x_L < x_0 < x_R$ (see Figure 6.1). In this chapter we let $\partial D = \partial D_c \cup \partial D_s$ where ∂D_s refers to the straight-line segment of the boundary and ∂D_c denotes the remaining curved part of ∂D. The distance between the interface and ∂D_c is assumed to be $O(1)$. In addition we assume that the distances from the interface to $(x_L, 0)$ and $(x_R, 0)$ are less than the distance from the interface to the rest of ∂D_c.

Near each end of the flat segment, it is assumed that the domain boundary can be represented by the graph of a function. Then near $(x_L, 0)$ as $x \to x_L^-$, ∂D can be written as $y = \psi_L(x)$. Similarly near $(x_R, 0)$ as $x \to x_R^+$, ∂D is given by $y = \psi_R(x)$. We assume that there exist constants K_L, $K_R \neq 0$, and α_L, $\alpha_R > 1$ such that

$$\psi_L'(x) \sim -K_L(x_L - x)^{\alpha_L}, \quad \text{as } x \to x_L^-, \tag{6.4a}$$

$$\psi_R'(x) \sim K_R(x - x_R)^{\alpha_R}, \quad \text{as } x \to x_R^+. \tag{6.4b}$$

When $\alpha_L = \alpha_R = 2$, then K_L and K_R are proportional to the curvature of the left and right ends of the straight-line segment respectively.

As in Chapter 5, the projection method [18] is used to determine the motion of the semi-circular interface. First, an equilibrium solution to (6.1a) with a semi-circular interface centered at $(x_0, 0)$ is found. We asymptotically analyze the eigenvalue problem associated with the linearization of (6.1) about the equilibrium solution. An explicit ordinary differential equation for the slow motion of the center of the interface, $x_0 = x_0(t)$, is then found using the projection method and the spectral information.

6.1 The Equilibrium Solution

To use the projection method, an equilibrium solution, $U_b(r;\epsilon)$ and $\sigma_b(\epsilon)$, to (6.1a) is required. This solution must have a semi-circular interface of radius $r = |\mathbf{x} - \mathbf{x}_0| = r_b$ centered at $\mathbf{x} = \mathbf{x}_0$. Such a solution is referred to as the canonical bubble solution [18] and is derived in Appendix A.1. We summarize the essential asymptotic properties of this equilibrium solution as $\epsilon \to 0$:

$$U_b(r;\epsilon) \sim \begin{cases} S_+(\epsilon) - a_+(r_b/r)^{1/2} e^{-\nu_+^\epsilon \epsilon^{-1}(r-r_b)}, & r > r_b, \\ u_0(\rho) + O(\epsilon), & \rho = \epsilon^{-1}(r - r_b) = O(1), \\ S_-(\epsilon) + a_-(r_b/r)^{1/2} e^{-\nu_-^\epsilon \epsilon^{-1}(r_b-r)}, & r < r_b, \end{cases} \tag{6.5}$$

$$\sigma_b(\epsilon) = \epsilon \frac{\beta}{(s_+ - s_-)r_b} + O(\epsilon^2). \tag{6.6}$$

Here $u_0(\rho)$ satisfies (A.4) and β is defined as

$$\beta \equiv \int_{-\infty}^{\infty} [u_0'(\rho)]^2 \, d\rho. \tag{6.7}$$

The values of the constants $S_\pm(\epsilon)$, $a_\pm$, and $\nu_\pm^\epsilon$ can be determined from (A.5), (A.9), and (A.11).

6.2 Spectral Estimates for the Linearized Problem

The eigenvalue problem associated with linearizing (6.1) about the canonical bubble solution $U_b(r;\epsilon)$ is given by

$$L_\epsilon \phi \equiv \epsilon^2 \Delta \phi + Q'[U_b(r;\epsilon)]\phi = \lambda \phi, \qquad \mathbf{x} \in D, \tag{6.8a}$$

$$\partial_n \phi = 0\,, \qquad \mathbf{x} \in \partial D\,, \tag{6.8b}$$

$$(\phi, \phi) = \int_D \phi^2 \, d\mathbf{x}\,. \tag{6.8c}$$

Here $(u, v) \equiv \int_D uv \, d\mathbf{x}$. The eigenvalues and eigenfunction of (6.8) are labeled by λ_j and ϕ_j respectively for $j = 0, 1, \ldots$, with $\lambda_j \to -\infty$ as $j \to \infty$.

The principal eigenfunction and eigenvalue for (6.8) are estimated in Appendix A.1 [18] and summarized below. The principal eigenvalue is given asymptotically by

$$\lambda_0(\epsilon) = \frac{\epsilon^2}{r_b} + O(\epsilon^3)\,. \tag{6.9}$$

The principal eigenfunction is estimated by

$$\phi_0 \sim \begin{cases} R_0 a_+ \nu_+^\epsilon (r_b/r)^{1/2} e^{-\nu_+^\epsilon \epsilon^{-1}(r - r_b)}\,, & r > r_b\,, \quad n = O(1)\,, \\ R_0 \left[u_0'(\rho) + \epsilon u_1'(\rho) + \epsilon^2 u_2'(\rho) + (\epsilon^3)\right]\,, & \rho = \epsilon^{-1}(r - r_b) = O(1)\,, \\ R_0 a_- \nu_-^\epsilon (r_b/r)^{1/2} e^{-\nu_-^\epsilon \epsilon^{-1}(r_b - r)}\,, & r < r_b\,. \end{cases} \tag{6.10}$$

In (6.10), $-n$ is the distance from $\mathbf{x} \in D$ to ∂D_c. The normalization constant, R_0, satisfies

$$R_0 \sim (\epsilon \pi r_b \beta)^{-1/2}\,. \tag{6.11}$$

To evaluate the boundary integrals below in §6.3, we use following estimate for ϕ_0 on ∂D near $(x_L, 0)$ and $(x_R, 0)$ for $r > r_b$:

$$\phi_0 \sim R_0 a_+ \nu_+^\epsilon (r_b/r)^{1/2} e^{-\nu_+^\epsilon \epsilon^{-1}(r - r_b)}\,. \tag{6.12}$$

This result is derived in Appendix A.2.

For this problem, the second eigenfunction corresponds to an exponentially small eigenvalue. This eigenfunction can be approximated by $\phi_1 \sim R_1 \partial_x U_b(r; \epsilon)$ where R_1 is a normalization constant. This function satisfies (6.8a) and fails to satisfy (6.8b) by only exponentially small terms. A boundary layer function can be added as in §5.2 to satisfy the boundary condition, but as in §5.2, this function has a negligible effect on the boundary integrals that are needed to be evaluated to determine the slow motion.

We use Green's identity on (6.8a) and $\partial_x U_b$ to estimate the second eigenvalue:

$$\lambda_1(\partial_x U_b, \phi_1) = -\epsilon^2 \int_{\partial D} \phi_1 \partial_n[\partial_x U_b]\, ds\,. \tag{6.13}$$

To estimate λ_1 we differentiate (6.5) to obtain that on ∂D for $r > r_b$,

$$\phi_1 \sim R_1 \partial_x U_b\,, \quad \text{where } \partial_x U_b \sim a_+ \nu_+^\epsilon \epsilon^{-1} (r_b/r)^{1/2} r^{-1} (x - x_0) e^{-\nu_+^\epsilon \epsilon^{-1}(r - r_b)}\,, \tag{6.14}$$

and

$$\partial_n[\partial_x U_b] \sim -a_+ (\nu_+^\epsilon)^2 \epsilon^{-2} (r_b/r)^{1/2} r^{-1} (x - x_0) e^{-\nu_+^\epsilon \epsilon^{-1}(r - r_b)} \hat{\mathbf{r}} \cdot \hat{\mathbf{n}}\,. \tag{6.15}$$

Here $\hat{\mathbf{n}}$ is the outward unit normal vector to ∂D and $\hat{\mathbf{r}} = (x - x_0, y)/r$ is a unit vector pointing from $(x_0, 0)$ to (x, y). To evaluate the left hand side of (6.13) Laplace's method is used as the dominant contribution to this integral arises in the region near $r = r_b$. Then using (6.5) we find

$$(\partial_x U_b, \phi_1) \sim \frac{\pi r_b \beta R_1}{2\epsilon}\,. \tag{6.16}$$

Since $\phi_1 \sim R_1 \partial_x U_b$, the normalization constant satisfies

$$R_1 \sim [2\epsilon/(\pi r_b \beta)]^{1/2}\,. \tag{6.17}$$

Substituting the results of (6.15), (6.16), and $\phi_1 \sim R_1 \partial_x U_b$ into (6.13) we obtain an asymptotic estimate for λ_1:

$$\lambda_1 \sim \frac{2a_+^2 (\nu_+^\epsilon)^3}{\pi \beta} \int_{\partial D} r^{-1} \left(\frac{x - x_0}{r}\right)^2 e^{-2\nu_+^\epsilon \epsilon^{-1}(r - r_b)} \hat{\mathbf{r}} \cdot \hat{\mathbf{n}}\, ds\,. \tag{6.18}$$

To evaluate the integral in (6.18) we notice that $\hat{\mathbf{r}} \cdot \hat{\mathbf{n}} = 0$ along ∂D_s. Because the integrand is exponentially decreasing for $r > r_b$ the dominant contribution to this integral comes from $O(\epsilon)$ regions near $(x_L, 0)$ and $(x_R, 0)$ where the boundary of the domain, ∂D, first starts to curve. We then use Laplace's method used to evaluate this integral. The following estimates are used near $(x_L, 0)$ as $x \to x_L^-$:

$$r \sim r_L - (x - x_L)\,, \quad \text{where } r_L \equiv x_0 - x_L \tag{6.19a}$$

$$\hat{\mathbf{r}} \sim (-1, 0)\,, \tag{6.19b}$$

$$\hat{\mathbf{n}} \sim \frac{(-K_L(x_L - x)^{\alpha_L}, -1)}{\left[K_L^2(x_L - x)^{2\alpha_L} + 1\right]^{1/2}}, \tag{6.19c}$$

$$ds \sim \left[K_L^2(x_L - x)^{2\alpha_L} + 1\right]^{1/2} dx\,. \tag{6.19d}$$

Similarly, near $(x_R, 0)$ as $x \to x_R^+$ we use

$$r \sim r_R + (x - x_R)\,, \quad \text{where } r_R \equiv x_R - x_0 \tag{6.20a}$$

$$\hat{\mathbf{r}} \sim (1, 0)\,, \tag{6.20b}$$

$$\hat{\mathbf{n}} \sim \frac{(K_R(x - x_R)^{\alpha_R}, -1)}{\left[K_R^2(x - x_R)^{2\alpha_R} + 1\right]^{1/2}}, \tag{6.20c}$$

$$ds \sim \left[K_R^2(x - x_R)^{2\alpha_R} + 1\right]^{1/2} dx\,. \tag{6.20d}$$

Here (6.4) was used to evaluate the outward unit normals into (6.19c) and (6.20c). We substitute (6.19) and (6.20) in (6.18) and apply Laplace's method to obtain

$$\lambda_1 \sim \frac{2a_+^2(\nu_+^\epsilon)^3}{\pi\beta}\left\{\frac{K_L}{x_0 - x_L}e^{-2\nu_+^\epsilon\epsilon^{-1}(x_0 - x_L - r_b)}I_L + \frac{K_R}{x_R - x_0}e^{-2\nu_+^\epsilon\epsilon^{-1}(x_R - x_0 - r_b)}I_R\right\}, \tag{6.21}$$

where

$$I_L = \int_{-\infty}^{x_L}(x_L - x)^{\alpha_L}e^{-2\nu_+^\epsilon\epsilon^{-1}(x_L - x)}\,dx\,, \tag{6.22a}$$

$$I_R = \int_{x_R}^{\infty}(x - x_R)^{\alpha_R}e^{-2\nu_+^\epsilon\epsilon^{-1}(x - x_R)}\,dx\,. \tag{6.22b}$$

The integrals I_L and I_R can be evaluated with a change of variables $\zeta = 2\nu_+^\epsilon\epsilon^{-1}(x_L - x)$ in (6.22a) and $\zeta = 2\nu_+^\epsilon\epsilon^{-1}(x - x_R)$ in (6.22b). Using this, we obtain

$$I_L = \left(\frac{\epsilon}{2\nu_+^\epsilon}\right)^{\alpha_L+1}\Gamma(\alpha_L + 1)\,, \tag{6.23a}$$

$$I_R = \left(\frac{\epsilon}{2\nu_+^\epsilon}\right)^{\alpha_R+1}\Gamma(\alpha_R + 1)\,. \tag{6.23b}$$

Thus, from the substitution (6.23) in (6.21), the exponentially small second eigenvalue is given by

$$\begin{aligned}\lambda_1 \;\sim\; & \frac{2a_+^2(\nu_+^\epsilon)^3}{\pi\beta}\left\{\frac{K_L}{x_0 - x_L}e^{-2\nu_+^\epsilon\epsilon^{-1}(x_0 - x_L - r_b)}\left(\frac{\epsilon}{2\nu_+^\epsilon}\right)^{\alpha_L+1}\Gamma(\alpha_L + 1)\right. \\ & \left. + \frac{K_R}{x_R - x_0}e^{-2\nu_+^\epsilon\epsilon^{-1}(x_R - x_0 - r_b)}\left(\frac{\epsilon}{2\nu_+^\epsilon}\right)^{\alpha_R+1}\Gamma(\alpha_R + 1)\right\}.\end{aligned} \tag{6.24}$$

6.3 The Projection Method

We apply the projection method to determine the motion of the semi-circular interface along the flat part of ∂D. The center of the semi-circle slowly slides along ∂D_s without change of shape until either a steady state is attained or the edge of the semi-circle first hits ∂D_c. The trajectory $x_0 = x_0(t)$, with $x_0(0) = x_0^0$, of the center of the circle is to be determined. It is assumed that the initial data is a canonical bubble solution $u(\mathbf{x},0) = U_b[|\mathbf{x} - \mathbf{x}_0^0|;\epsilon]$ with $\sigma = \sigma_b(\epsilon)$, and $\mathbf{x}_0^0 = (x_0^0, 0)$. We set $u(\mathbf{x},t) = U_b[|\mathbf{x} - \mathbf{x}_0|;\epsilon] + w(\mathbf{x},t)$ and $\sigma(t) = \sigma_b + \mu(t)$. Linearizing (6.1) about U_b, and assuming that $w \ll U_b$ and $\mu \ll \sigma_b$ uniformly in time, we produce

$$L_\epsilon w \equiv \epsilon^2 \Delta w + Q'(U_b) w = \partial_t U_b + \mu\,, \qquad \mathbf{x} \in D\,, \tag{6.25a}$$

$$\partial_n w = -\partial_n U_b, \qquad \mathbf{x} \in \partial D\,. \tag{6.25b}$$

$$\int_D w\, d\mathbf{x} = 0\,. \tag{6.25c}$$

Next, we expand $w = \sum_{j=0}^{\infty} c_j \phi_j/\lambda_j$ in terms of the eigenfunctions of (6.8). Integrating by parts produces

$$(\phi_j, L_\epsilon w) - (w, L_\epsilon \phi_j) = (\phi_j, \partial_t U_b) + (\phi_j, \mu) - \lambda_j (w, \phi_j)\,. \tag{6.26}$$

Applying Green's identity to (6.26) and using $\lambda_j(w,\phi_j) = c_j$ we determine that the coefficients c_j for $j = 0, 1, \ldots,$ satisfy

$$c_j = (\phi_j, \partial_t U_b) + \mu(\phi_j, 1) + \epsilon^2 \int_{\partial D} \phi_j \partial_n U_b\, ds\,. \tag{6.27}$$

In order to satisfy (6.25c), we also need that

$$\sum_{j=0}^{\infty} \frac{c_j}{\lambda_j}(\phi_j, 1) = 0\,. \tag{6.28}$$

To guarantee that $w \ll U_b$ on an $O(\epsilon^{-2})$ time scale we need $c_0 = 0$ since $\lambda_0 = O(\epsilon^2)$. Similarly, we also require that $c_1 = 0$ to prevent growth on exponentially long time intervals since λ_1, as in (6.24), is exponentially small. Thus we have the following two coupled solvability conditions

which will determine $x_0(t)$ and $\mu(t)$:

$$(\phi_0, \partial_t U_b) + \mu(\phi_0, 1) + \epsilon^2 \int_{\partial D} \phi_0 \partial_n U_b \, ds = 0 \,, \tag{6.29a}$$

$$(\phi_1, \partial_t U_b) + \mu(\phi_1, 1) + \epsilon^2 \int_{\partial D} \phi_1 \partial_n U_b \, ds = 0 \,. \tag{6.29b}$$

These two equations can be decoupled as follows. First, from (6.10), (6.11), (6.14), (6.17), and (6.34) it can be seen that the two boundary integral terms in (6.29) have the same asymptotic order as $\epsilon \to 0$. Next, since ϕ_0 is even while ϕ_1 is odd in $x - x_0$, it follows from the exponential decay of both eigenfunctions for $r > r_b$ that $(\phi_0, 1)$ is exponentially larger than $(\phi_1, 1)$. Finally, a similar symmetry argument can be used to show that $(\phi_0, \partial_t U_b)$ is exponentially smaller than $(\phi_1, \partial_t U_b)$. Therefore, we can neglect $(\phi_0, \partial_t U_b)$ in (6.29a) and $\mu(\phi_1, 1)$ in (6.29b). This yields the following two uncoupled problems for μ and $x_0(t)$ respectively:

$$\mu(\phi_0, 1) \sim -\epsilon^2 \int_{\partial D} \phi_0 \partial_n U_b \, ds \,, \tag{6.30a}$$

$$(\phi_1, \partial_t U_b) \sim -\epsilon^2 \int_{\partial D} \phi_1 \partial_n U_b \, ds \,. \tag{6.30b}$$

The terms in (6.30) are evaluated next. Recalling that ϕ_0 is localized near $r = r_b$ and using (6.10), we calculate that

$$(\phi_0, 1) \sim \epsilon \pi R_0 r_b (s_+ - s_-) \,. \tag{6.31}$$

To evaluate $(\phi_1, \partial_t U_b)$ we use $\partial_t U_b = -U_b' \left(\frac{x - x_0}{r}\right) x_0'(t)$, $\phi_1 \sim R_1 \partial_x U_b$, and note that the dominant contribution to this integral also arises from the region near $r = r_b$. Then

$$(\phi_1, \partial_t U_b) \sim -x_0'(t) R_1 \int_D [U_b']^2 \left(\frac{x - x_0}{r}\right)^2 d\mathbf{x} \sim -x_0'(t) \frac{R_1 r_b}{\epsilon} \int_0^{\pi} \int_{-\infty}^{\infty} [u_0'(\rho)]^2 \cos^2(\theta) \, d\rho \, d\theta \,. \tag{6.32}$$

Thus,

$$(\phi_1, \partial_t U_b) \sim -x_0'(t) \frac{R_1 r_b \pi \beta}{2\epsilon} \,, \tag{6.33}$$

where β is defined in (6.7). To evaluate the right sides of (6.30) we use (6.5) to obtain that, for $r > r_b$ on ∂D,

$$\partial_n U_b \sim a_+ \nu_+^{\epsilon} \epsilon^{-1} (r_b / r)^{1/2} e^{-\nu_+^{\epsilon} \epsilon^{-1} (r - r_b)} \hat{\mathbf{r}} \cdot \hat{\mathbf{n}} \,. \tag{6.34}$$

Then by substituting (6.31), (6.33), (6.34), (6.10), and (6.14) into (6.30) we obtain the slow motion equations:

$$\mu(t) \sim -\frac{a_+^2(\nu_+^\epsilon)^2}{\pi(s_+ - s_-)} \int_{\partial D} r^{-1} e^{-2\nu_+^\epsilon \epsilon^{-1}(r-r_b)} \hat{\mathbf{r}} \cdot \hat{\mathbf{n}}\, ds\,, \tag{6.35a}$$

$$x_0'(t) \sim \frac{2\epsilon a_+^2(\nu_+^\epsilon)^2}{\pi\beta} \int_{\partial D} r^{-1} \frac{x - x_0}{r} e^{-2\nu_+^\epsilon \epsilon^{-1}(r-r_b)} \hat{\mathbf{r}} \cdot \hat{\mathbf{n}}\, ds\,. \tag{6.35b}$$

Since the dominant contribution to the integrals in (6.35) arises from the regions near $(x_L, 0)$ and $(x_R, 0)$, we can estimate them using a Laplace type argument similar to that used to calculate (6.21). Substituting the estimates written in (6.19) and (6.20) into (6.35) we get

$$\mu(t) \sim -\frac{a_+^2(\nu_+^\epsilon)^2}{\pi(s_+ - s_-)} \left\{ \frac{K_L}{x_0 - x_L} e^{-2\nu_+^\epsilon \epsilon^{-1}(x_0 - x_L - r_b)} I_L + \frac{K_R}{x_R - x_0} e^{-2\nu_+^\epsilon \epsilon^{-1}(x_R - x_0 - r_b)} I_R \right\} \tag{6.36a}$$

$$x_0'(t) \sim \frac{2\epsilon a_+^2(\nu_+^\epsilon)^2}{\pi\beta} \left\{ \frac{K_R}{x_R - x_0} e^{-2\nu_+^\epsilon \epsilon^{-1}(x_R - x_0 - r_b)} I_R - \frac{K_L}{x_0 - x_L} e^{-2\nu_+^\epsilon \epsilon^{-1}(x_0 - x_L - r_b)} I_L \right\} \tag{6.36b}$$

Here I_L and I_R are defined in (6.22). Finally, the result of (6.23) is used in (6.36) to obtain the slow motion result:

$$\begin{aligned} \mu(t) \;\sim\; & -\frac{a_+^2(\nu_+^\epsilon)^2}{\pi(s_+ - s_-)} \left\{ \frac{K_L}{x_0 - x_L} e^{-2\nu_+^\epsilon \epsilon^{-1}(x_0 - x_L - r_b)} \left(\frac{\epsilon}{2\nu_+^\epsilon} \right)^{\alpha_L + 1} \Gamma(\alpha_L + 1) \right. \\ & \left. + \frac{K_R}{x_R - x_0} e^{-2\nu_+^\epsilon \epsilon^{-1}(x_R - x_0 - r_b)} \left(\frac{\epsilon}{2\nu_+^\epsilon} \right)^{\alpha_R + 1} \Gamma(\alpha_R + 1) \right\}, \end{aligned} \tag{6.37a}$$

$$\begin{aligned} x_0'(t) \;\sim\; & \frac{2\epsilon a_+^2(\nu_+^\epsilon)^2}{\pi\beta} \left\{ \frac{K_R}{x_R - x_0} e^{-2\nu_+^\epsilon \epsilon^{-1}(x_R - x_0 - r_b)} \left(\frac{\epsilon}{2\nu_+^\epsilon} \right)^{\alpha_R + 1} \Gamma(\alpha_R + 1) \right. \\ & \left. - \frac{K_L}{x_0 - x_L} e^{-2\nu_+^\epsilon \epsilon^{-1}(x_0 - x_L - r_b)} \left(\frac{\epsilon}{2\nu_+^\epsilon} \right)^{\alpha_L + 1} \Gamma(\alpha_L + 1) \right\}. \end{aligned} \tag{6.37b}$$

Referring to the ODE (6.37b), for $x_0(t)$, we see that the motion of the center of the semi-circular interface along the straight-line boundary segment between $(x_L, 0)$ and $(x_R, 0)$ is determined by the shape of the boundary at $(x_L, 0)$ and $(x_R, 0)$ and the distance from the interface to these points. The interface will move. according to (6.37b), without change of shape until a stable steady state is reached or until the interface touches $(x_L, 0)$ or $(x_R, 0)$. If the interface reaches the curved part of the boundary, it will subsequently continue to evolve according to (6.3).

6.4 Steady States

We can find steady state locations for the center of the semi-circular interface between $(x_L, 0)$ and $(x_R, 0)$. These steady state locations are the values of x_0 for which $x_0'(t) = 0$. From (6.37b), a steady state x_0^e must satisfy

$$\frac{x_0^e - x_L}{x_R - x_0^e} e^{4\nu_+^\epsilon \epsilon^{-1} x_0^e} = \frac{K_L \Gamma(\alpha_L + 1)}{K_R \Gamma(\alpha_R + 1)} \left(\frac{\epsilon}{2\nu_+^\epsilon} \right)^{\alpha_L - \alpha_R} e^{2\nu_+^\epsilon \epsilon^{-1}(x_R + x_L)} . \tag{6.38}$$

Since the left side of (6.38) increases from 0 to ∞ as x_0^e goes from x_L to x_R, a unique steady state exists whenever K_L and K_R are of the same sign. This steady state is stable when K_L, $K_R < 0$, and unstable when K_L, $K_R > 0$. In particular, this implies that if D is convex near $(x_L, 0)$ and $(x_R, 0)$, then there is no stable equilibrium location on ∂D_s. Expanding $x_0^e = \sum_{j=0}^{\infty} \epsilon^j x_{0j}^e$ in (6.38) and solving up to second order, we obtain that

$$x_0^e \sim \frac{x_L + x_R}{2} + \frac{\epsilon}{4\nu_+^\epsilon} \log \left[\frac{K_L \Gamma(\alpha_L + 1)}{K_R \Gamma(\alpha_R + 1)} \left(\frac{\epsilon}{2\nu_+^\epsilon} \right)^{\alpha_L - \alpha_R} \right] + O(\epsilon^2) . \tag{6.39}$$

Thus, the equilibrium location, x_0^e is located at an $O(\epsilon)$ distance from the midpoint of the straight-line boundary segment.

6.5 Examples of Slow Dynamics

As an example, the following form was examined for $Q(u)$:

$$Q(u) = 2(u - u^3) . \tag{6.40}$$

Using (A.4a), (A.5), (A.9b) and (A.11), the constants $\nu_\pm^\epsilon$, $a_\pm$, $s_\pm$, and β satisfy

$$\nu_\pm^\epsilon = 2[1 - \epsilon(4r_b)^{-1} + \cdots] , \quad a_\pm = 2 , \quad s_\pm = \pm 1 , \quad \beta = 4/3 . \tag{6.41}$$

We consider the case when $\alpha_L = \alpha_R = \alpha$. In this situation, the ODE for the center of the semi-circular interface, (6.37b), is given by

$$x_0' \sim \frac{6\epsilon^{\alpha+2}\Gamma(\alpha + 1)}{4^\alpha \pi} \left[\frac{K_R}{x_R - x_0} e^{-2\nu_+^\epsilon \epsilon^{-1}(x_R - x_0 - r_b)} - \frac{K_L}{x_0 - x_L} e^{-2\nu_+^\epsilon \epsilon^{-1}(x_0 - x_L - r_b)} \right] . \tag{6.42}$$

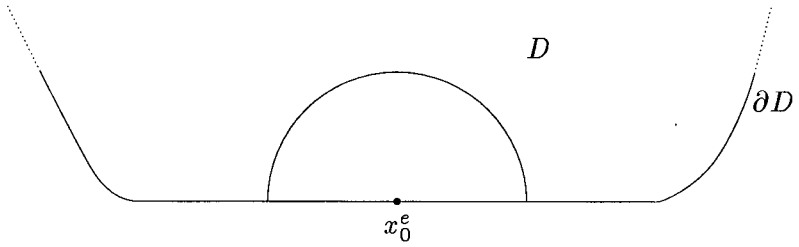

Figure 6.2: Plot of part of a domain boundary, ∂D, upon which the center of the semi-circular interface is at an unstable steady state. K_L, $K_R > 0$ for this domain.

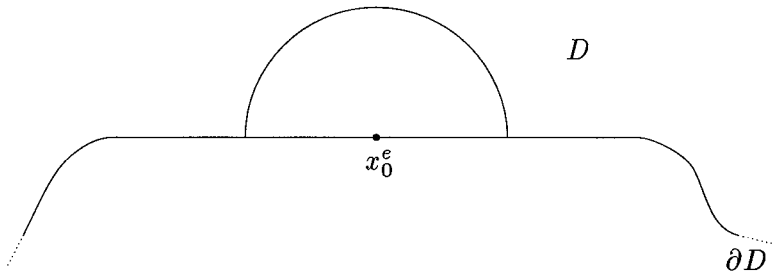

Figure 6.3: Plot of part of a domain boundary, ∂D, upon which the center of the semi-circular interface is at a stable steady state. K_L, $K_R < 0$ for this domain.

The steady state location for x_0, assuming that K_L and K_R have the same sign, is

$$x_0^e \sim \frac{x_L + x_R}{2} + \frac{\epsilon}{8} \log\left(\frac{K_L}{K_R}\right). \tag{6.43}$$

Assume that the initial location of the center of the semi-circular interface is $x_0(0) = x_0^0$. Then the following motion can be deduced from (6.42) and (6.43). When $K_L > 0$ and $K_R > 0$, $x_0(t)$ will move monotonically towards x_L if $x_0^0 < x_0^e$, or monotonically towards x_R if $x_0^0 > x_0^e$. (See Figure 6.2.) When $K_L < 0$ and $K_R < 0$, $x_0(t)$ will approach the stable steady state at x_0^e. (See Figure 6.3.) If $K_L < 0$ and $K_R > 0$, then $x_0(t)$ will move towards x_R. (See Figure 6.4.) Similarly, $x_0(t)$ will move towards x_L if $K_L > 0$ and $K_R < 0$. When the interface touches $(x_L, 0)$ or $(x_R, 0)$, the subsequent evolution of the interface is determined by (6.3).

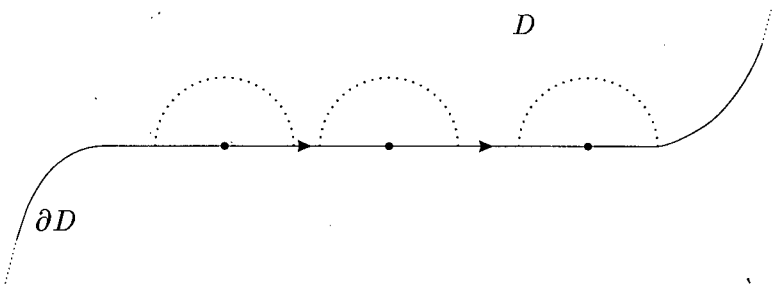

Figure 6.4: Plot of part of a domain boundary, ∂D, upon which the center of the semi-circular interface moves toward the right. $K_L < 0$ and $K_R > 0$ for this domain.

Chapter 7

Summary

In this thesis we have asymptotically and numerically analyzed the Allen-Cahn equation with a mass constraint in a two-dimensional domain. Using the method of matched asymptotic expansions with multiple time scales, we have shown that solutions to the Allen-Cahn equation quickly develop internal layers, or interfaces, separating regions in which the solution is constant. These interfaces evolve satisfying the area preserving mean curvature flow, equation (1.4). Small approximately semi-circular interfaces intersecting the domain boundary were shown to asymptotically satisfy the ODE (1.6), and move along the boundary in the direction of increasing boundary curvature. A numerical method for simulating the motion of interfaces was presented. Using this method, we numerically verified asymptotic results including the small drop result, (1.6). The projection method was introduced and used to solve a metastable problem for the unconstrained Allen-Cahn equation. Finally, the projection method was used to determine the motion of a semi-circular interface intersecting a straight-line domain boundary segment between $(x_L, 0)$ and $(x_R, 0)$. It was found that the center of such a semi-circular interface satisfied the asymptotic ODE given by (1.7).

Bibliography

[1] N. Alikakos, X. Chen, G. Fusco, *Motion of a Drop by Surface Tension Along the Boundary*, preprint.

[2] N. Alikakos, G. Fusco, *Some Aspects of the Dynamics of the Cahn-Hilliard Equation*, Resenhas Vol. 1 No. 4, (1994), pp. 517-530.

[3] N. Alikakos, G. Fusco, M. Kowalczyk, *Finite Dimensional Dynamics and Interfaces Intersecting the Boundary I*, preprint.

[4] U. Ascher, *CPSC 542 Course Notes*, unpublished.

[5] C. M. Bender, S. A. Orszag, *Advanced Mathematical Methods for Scientists and Engineers*, McGraw-Hill, New York, (1978).

[6] R. L. Burden, J. D. Faires, *Numerical Analysis, Fifth Edition*,PWS Publishing Co., Boston, (1993).

[7] L. Bronsard, B. Wetton, *A Numerical Method for Tracking Curve Networks Moving with Curvature Motion*, J. Comp. Phys. 120 No. 1, (1995), pp. 66-87.

[8] G. Caginalp, P.C. Fife, *Dynamics of Layered Interfaces Arising From Phase Boundaries*, SIAM J. Appl. Math. Vol. 48, No. 3, (1988), pp. 506-518.

[9] M. Gage, *On an Area-Preserving Evolution For Plane Curves*, Contemp. Math. 51, (1986), pp. 51-62.

[10] M. Gage, R.S. Hamilton, *The Heat Equation Shrinking Convex Plane Curves*, J. Diff. Geom. 23, (1986), pp. 69-96.

[11] C. C. Hsiung, *A First Course in Differential Geometry*, Wiley Interscience Series in Pure and Applied Mathematics, New York, (1981).

[12] M. Kowalczyk, *Exponentially Slow Dynamics and Interfaces Intersecting the Boundary*, preprint.

[13] J. Rubinstein, P. Sternberg, *Nonlocal Reaction-Diffusion Equations and Nucleation*, IMA J. Appl. Math. Vol. 48, (1992), pp. 249-264.

[14] J. Rubinstein, P. Sternberg, J. Keller, Fast Reaction, Slow Diffusion, and Curve Shortening, SIAM J. Appl. Math. Vol. 49, No. 1, (1989), pp. 116-133.

[15] S. Ruuth, *An Algorithm for Generating Motion by Mean Curvature*, in Proc. 12th International Conference on Analysis and Optimization of Systems Images Wavelets and PDE's, Paris, June 26-28 1996, pp. 82-91.

[16] B. Seymour, *Math 550 Course Notes*, unpublished.

[17] M. J. Ward, *Dynamic Metastability and Singular Perturbations*, to appear in AMS book "Boundaries, Interfaces and Transitions".

[18] M. J. Ward, *Metastable Bubble Solutions for the Allen-Cahn Equation with Mass Conservation*, SIAM J. Appl. Math. Vol. 56, No. 5, (1996), pp. 1247–1279.

[19] M. J. Ward, *Math 551 Course Notes*, unpublished.

Appendix A

Asymptotic Estimates for the Constrained Allen-Cahn Equation

This appendix summarizes some of the calculations done in [18] needed in this thesis.

A.1 The Canonical Bubble Solution

In this appendix, the canonical bubble solution is derived. As $\epsilon \to 0$, this is an equilibrium solution to (6.1a) in $[-\infty, \infty] \times [0, \infty]$ with one radially symmetric interface of radius $r = r_b$ centered at $(x_0, 0)$. The functions $U_b(r;\epsilon)$ and $\sigma_b(\epsilon)$, called the canonical bubble solution, satisfy

$$\epsilon^2 \Delta U_b + Q(U_b) = \sigma_b\,, \qquad 0 < r < \infty\,; \qquad U_b' > 0\,, \tag{A.1a}$$

$$U_b(r_b;\epsilon) = 0\,; \qquad U_b(r;\epsilon) \to S_\pm(\epsilon) \quad \text{as } \epsilon^{-1}(r - r_b) \to \pm\infty\,. \tag{A.1b}$$

Here $S_\pm(\epsilon)$ are defined as the roots of

$$Q[S_\pm(\epsilon)] = \sigma_b(\epsilon)\,, \tag{A.2}$$

for which $S_\pm(\epsilon) \to s_\pm$ and $\sigma_b(\epsilon) \to 0$ as $\epsilon \to 0$. The method of matched asymptotic expansions is used to construct the solution.

In the inner region near the interface, $\rho \equiv \epsilon^{-1}(r - r_b) = O(1)$ and we denote $u_b(\rho;\epsilon) = U_b(r_b + \epsilon\rho;\epsilon)$. From (A.1) we obtain

$$u_b'' + \frac{\epsilon}{r_b + \epsilon\rho} u_b' + Q(u_b) = \sigma_b\,, \qquad -\infty < \rho < \infty\,; \qquad u_b' > 0\,, \tag{A.3a}$$

$$u_b(0;\epsilon) = 0\,; \qquad u_b(\rho;\epsilon) \to S_\pm(\epsilon) \quad \text{as } \rho \to \pm\infty\,. \tag{A.3b}$$

Then to leading order as $\epsilon \to 0$ we have that $S_\pm(\epsilon) \to s_\pm$, $\sigma_b(\epsilon) \to 0$, and $u_b(\rho;\epsilon) \to u_0(\rho)$,

where $u_0(\rho)$ satisfies

$$u_0'' + Q(u_0) = 0\,, \qquad -\infty < \rho < \infty\,; \qquad u_0' > 0\,, \qquad u_0(0;\epsilon) = 0\,, \tag{A.4a}$$

$$u_0(\rho) \sim s_+ - a_+ e^{-\nu_+ \rho} \quad \rho \to \infty\,; \qquad u_0(\rho) \sim s_- + a_- e^{\nu_- \rho} \quad \rho \to -\infty\,. \tag{A.4b}$$

Here the positive constants $\nu_\pm$ and $a_\pm$ are defined by

$$\nu_\pm = [-Q'(s_\pm)]^{1/2}\,, \qquad \log a_\pm = \log(\pm s_\pm) + \int_0^{s_\pm} \left(\frac{\pm \nu_\pm}{[2V(\eta)]^{1/2}} + \frac{1}{\eta - s_\pm} \right) d\eta\,, \tag{A.5}$$

where $V(u) \equiv -\int_{s_-}^{u} Q(\eta)\, d\eta$.

We expand the solution to (A.3) as

$$u_b(\rho;\epsilon) \sim \sum_{j=0}^{\infty} \epsilon^j u_j(\rho)\,, \qquad \sigma_b(\epsilon) \sim \sum_{j=1}^{\infty} \epsilon^j \sigma_j\,, \qquad S_\pm(\epsilon) \sim s_\pm + \sum_{j=1}^{\infty} \epsilon^j u_j(\pm\infty)\,. \tag{A.6}$$

Substituting (A.6) into (A.3) we obtain for some functions $G_j(u_0, \ldots, u_{j-1})$ and $g_{j\pm}(\sigma_1, \ldots, \sigma_{j-1})$, that u_j for $j \geq 1$ satisfies

$$Lu_j \equiv u_j'' + Q'(u_0) u_j = \sigma_j + G_j(u_0, \ldots, u_{j-1})\,, \qquad -\infty < \rho < \infty\,; \tag{A.7a}$$

$$u_j(\rho) \to -\sigma_j \nu_\pm^{-2} + g_{j\pm}(\sigma_1, \ldots, \sigma_{j-1})\,, \quad \text{as } \rho \to \pm\infty\,; \qquad u_j(0) = 0\,. \tag{A.7b}$$

From (A.4a) we see that $Lu_0' = 0$ and $u_0'(\pm\infty) = 0$. Thus the right side of (A.7a) produces a solvability condition that determines σ_j as

$$\sigma_j = \frac{-1}{s_+ - s_-} \int_{-\infty}^{\infty} u_0' G_j(u_0, \ldots, u_{j-1})\, d\rho\,, \quad \text{for } j \geq 1\,. \tag{A.8}$$

Equations (A.7) and (A.8) determine the asymptotic expansions for $u_b(\rho;\epsilon)$, $\sigma_b(\epsilon)$, and $S_\pm(\epsilon)$. These conditions give

$$S_\pm(\epsilon) = s_\pm - \epsilon \sigma_1 \nu_\pm^{-2} + O(\epsilon^2)\,, \tag{A.9a}$$

$$\sigma_1 = \frac{\beta}{(s_+ - s_-) r_b}\,, \quad \text{where } \beta \equiv \int_{-\infty}^{\infty} [u_0'(\rho)]^2\, d\rho = \sqrt{2} \int_{s_-}^{s_+} [V(u)]^{1/2}\, du\,. \tag{A.9b}$$

In the outer region for $r > r_b$ we write $U_b(r;\epsilon) = S_+(\epsilon) + u_+(r;\epsilon)$, where $u_+ \ll S_+$. Similarly, in the region where $r < r_b$ we use $U_b(r;\epsilon) = S_-(\epsilon) + u_-(r;\epsilon)$, where $u_- \ll S_-$. We linearize

(A.1a) about $S_\pm$ to obtain that

$$u_+'' + r^{-1}u_+' - (\epsilon^{-1}\nu_+^\epsilon)^2 u_+ = 0\,, \quad r > r_b\,, \tag{A.10a}$$

$$u_-'' + r^{-1}u_-' - (\epsilon^{-1}\nu_-^\epsilon)^2 u_- = 0\,, \quad r < r_b\,. \tag{A.10b}$$

Here $\nu_\pm^\epsilon = (-Q'[S_\pm(\epsilon)])^{1/2}$. Then using (A.9a) we have

$$\nu_\pm^\epsilon = \nu_\pm \left[1 + \frac{\epsilon\sigma_1}{2\nu_\pm^4} Q''(s_\pm) + O(\epsilon^2)\right]. \tag{A.11}$$

Equations (A.10) can be solved exactly in terms of K_m, the modified Bessel function of the second kind of order m, and I_m, the modified Bessel function of the first kind, respectively. These can be estimated asymptotically using large argument expansions. Matching this to the inner solution in (A.4) produces

$$U_b(r;\epsilon) \sim \begin{cases} S_+(\epsilon) - a_+(r_b/r)^{1/2} e^{-\nu_+^\epsilon \epsilon^{-1}(r-r_b)}\,, & r > r_b\,, \\ \sum_{j=0}^\infty \epsilon^j u_j(\rho)\,, & \rho = \epsilon^{-1}(r-r_b) = O(1)\,, \\ S_-(\epsilon) + a_-(r_b/r)^{1/2} e^{-\nu_-^\epsilon \epsilon^{-1}(r_b-r)}\,, & r < r_b\,. \end{cases} \tag{A.12}$$

A.2 The Principal Eigenpair

This appendix summarizes the calculations done in [18] to asymptotically estimate the principal eigenfunction, ϕ_0, and eigenvalue, λ_0, for the eigenvalue problem (6.8). The principal eigenfunction is radially symmetric except in an $O(\epsilon)$ region near the curved part of ∂D.

In the internal layer region we set $\rho = \epsilon^{-1}(r - r_b)$ and $\Phi_0(\rho;\epsilon) = \phi_0(r_b + \epsilon\rho)$. The following expansions are used as $\epsilon \to 0$:

$$\Phi_0(\rho;\epsilon) \sim \sum_{j=0}^\infty \epsilon^j \Phi_{0j}\,, \qquad \lambda_0(\epsilon) \sim \sum_{j=0}^\infty \epsilon^j \lambda_{0j}(\rho)\,, \tag{A.13a}$$

$$Q'(U_b) = Q_0' + (\epsilon u_1 + \epsilon^2 u_2) Q_0'' + \frac{\epsilon^2}{2} u_1^2 Q_0'' + \cdots. \tag{A.13b}$$

Here $Q_0' \equiv Q_0'(u_0)$, $Q_0'' \equiv Q_0''(u_0)$, etc, and from (A.12), $U_b(r;\epsilon) \sim \sum_{j=0}^\infty \epsilon^j u_j(\rho)$ in this region. Substituting (A.13a) into (6.8) and collecting powers of ϵ we produce

$$L\Phi_{00} \;=\; \lambda_{00}\Phi_{00}\,, \tag{A.14a}$$

$$L\Phi_{01} = -u_1\Phi_{00}Q_0'' - r_b^{-1}\Phi_{00}' + \lambda_{01}\Phi_{00} + +\lambda_{00}\Phi_{01}\,, \tag{A.14b}$$

$$L\Phi_{02} = -r_b^{-1}\Phi_{01}' + \rho r_b^{-2}\Phi_{00}' - u_1\Phi_{01}Q_0'' - u_2\Phi_{00}Q_0'' - \frac{1}{2}u_1^2\Phi_{00}Q_0'' + \lambda_{00}\Phi_{02} + \lambda_{01}\Phi_{01} + \lambda_{02}\Phi_{00}\,. \tag{A.14c}$$

In (A.14), Lv is defined in (A.7a) and we need $\Phi_{0j}(\rho) \to 0$ as $\rho \to \pm\infty$. Since $Lu_0' = 0$ and $u_0'(\pm\infty) = 0$, we have the solvability condition that $L\Phi_{0j}$ for $j = 0, 1, 2$ is orthogonal to u_0'. This solvability condition is used to determine Φ_{0j} and λ_{0j} for $j = 0, 1, 2$. The results are

$$\Phi_0(\rho;\epsilon) = R_0\left[u_0'(\rho) + \epsilon u_1'(\rho) + \epsilon^2 u_2'(\rho) + O(\epsilon^3)\right]\,, \tag{A.15}$$

$$\lambda_0 = \epsilon^2 r_b^{-1} + O(\epsilon^3)\,, \tag{A.16}$$

where R_0 is a normalization constant.

In the outer regions we let $\phi_0 \sim R_0\phi_+(r;\epsilon)$ and $\phi_0 \sim R_0\phi_-(r;\epsilon)$ for $r > r_b$ and $r < r_b$ respectively. The eigenvalue problem (6.8) becomes

$$\phi_+'' + r^{-1}\phi_+' - (\epsilon^{-1}\tilde{\nu}_+^\epsilon)^2\phi_+ = 0\,, \quad r > r_b\,, \tag{A.17a}$$

$$\phi_-'' + r^{-1}\phi_-' - (\epsilon^{-1}\tilde{\nu}_-^\epsilon)^2\phi_- = 0\,, \quad r < r_b\,. \tag{A.17b}$$

Here we have defined $\tilde{\nu}_\pm^\epsilon \equiv \nu_\pm^\epsilon[1 + \lambda_0/(\nu_\pm^\epsilon)^2]^{1/2}$. These equations can be solved and matched to (A.15), to produce

$$\phi_0 \sim \begin{cases} R_0 a_+ \nu_+^\epsilon (r_b/r)^{1/2} e^{-\nu_+^\epsilon \epsilon^{-1}(r-r_b)}\,, & r > r_b\,, \quad n = O(1)\,, \\ R_0\left[u_0'(\rho) + \epsilon u_1'(\rho) + \epsilon^2 u_2'(\rho) + (\epsilon^3)\right]\,, & \rho = \epsilon^{-1}(r - r_b) = O(1)\,, \\ R_0 a_- \nu_-^\epsilon (r_b/r)^{1/2} e^{-\nu_-^\epsilon \epsilon^{-1}(r_b-r)}\,, & r < r_b\,. \end{cases} \tag{A.18}$$

In (A.18) $-n$ is the distance from $\mathbf{x} \in D$ to ∂D_c. The normalization constant R_0 is calculated asymptotically to be

$$R_0 \sim (\epsilon\pi r_b\beta)^{-1/2}\,. \tag{A.19}$$

To satisfy the boundary condition (6.8b) we need to add to (A.18) an exponentially small boundary layer function. This calculation was done in [18] where it was shown that on ∂D, ϕ_0 satisfies

$$\phi_0 \sim R_0 a_+ \nu_+^\epsilon (r_b/r)^{1/2} e^{-\nu_+^\epsilon \epsilon^{-1}(r-r_b)}[1 + \hat{\mathbf{r}}\cdot\hat{\mathbf{n}}]\,. \tag{A.20}$$

To evaluate the boundary integrals in §6.3, we need an estimate for ϕ_0 on ∂D near $(x_L, 0)$ and $(x_R, 0)$. Using (6.19) and (6.20) we obtain to leading that on ∂D and near the corner points $(x_L, 0)$ and $(x_R, 0)$, ϕ_0 satisfies

$$\phi_0 \sim R_0 a_+ \nu_+^\epsilon (r_b/r)^{1/2} e^{-\nu_+^\epsilon \epsilon^{-1}(r-r_b)}. \tag{A.21}$$